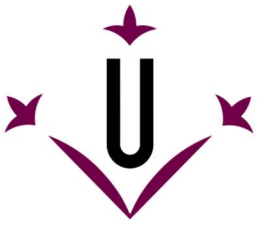

THE JOURNAL OF Pathology
A Journal of The Pathological So
Understanding

# Cytoplasmic Cyclin D1 regulates glioblastoma dissemination

| | |
|---|---|
| Journal: | *The Journal of Pathology* |
| Manuscript ID | 18-721.R2 |
| Wiley - Manuscript type: | Original Research Article |
| Date Submitted by the Author: | n/a |
| Complete List of Authors: | Cemeli, Tània; University of Lleida. IRBLleida, Basical Medical Sciences<br>Guasch, Marta; University of Lleida. IRBLleida, Basical Medical Sciences<br>Nàger, Mireia; University of Lleida. IRBLleida, Basical Medical Sciences; Institute of Medical Biology, Molecular Cancer Research Group<br>Felip, Isidre; University of Lleida. IRBLleida, Basical Medical Sciences<br>Cambray, Serafi; University of Lleida. IRBLleida, Basical Medical Sciences<br>Santacana, Maria; IRB-Lleida, Oncologic Pathology group<br>Gatius, Sònia ; University of Lleida. IRBLleida, Basical Medical Sciences<br>Pedraza, Neus; University of Lleida. IRBLleida, Basical Medical Sciences<br>Dolcet, Xavier; Universitat de Lleida/Institut de Recerca Biomèdica de Lleida, Department of Ciencies Mediques Basiques;<br>Ferrezuelo, Francisco; University of Lleida. IRBLleida, Basical Medical Sciences<br>Schuhmacher, Alberto; Aragon Health Research Institute , Biomedical Research<br>Herreros, Judith; University of Lleida. IRBLleida, Basical Medical Sciences<br>GARI, ELOI; University of Lleida. IRBLleida, Basical Medical Sciences |
| Tissue: | |
| Pathology: | |
| Technique: | |
| | |

# Cytoplasmic Cyclin D1 regulates glioblastoma dissemination

Tània Cemeli[1], Marta Guasch[1], Mireia Nàger[2§], Isidre Felip[3], Serafí Cambray[4], Maria Santacana[5], Sònia Gatius[5], Neus Pedraza[1], Xavier Dolcet[3], Francisco Ferrezuelo[1], Alberto J. Schuhmacher[6], Judit Herreros[2], Eloi Garí[1*]

Cell Cycle[1], Calcium Signaling[2], Oncological Pathology[3] and Vascular and Renal Translational[4] Groups of the Institut de Recerca Biomèdica de Lleida (IRBLLEIDA), Department of Basic Medical Sciences at University of Lleida, and Department of Pathology and Molecular Genetics at Hospital Universitari Arnau de Vilanova (HUAV)[5], Lleida, Catalonia, Spain.

[6]Biomedical Research Center of Aragon. Aragon Health Research Institute (IIS Aragón), Zaragoza, Spain.

[§]Present address: Molecular Cancer Research Group, Institute of Medical Biology, University of Tromsø - The Arctic University of Norway, 9037 Tromsø, Norway.

***Correspondence**: Eloi Garí. Institut de Recerca Biomèdica de Lleida (IRBLleida) Av. Alcalde Rovira Roure 80, 25198, Lleida, Catalonia. Spain. Phone: +34973702414. E-mail: eloi.gari@cmb.udl.cat

**Running title:** Ccnd1-dependent GBM spread

**Conflicts of Interest**

The authors have declared no conflicts of interest.

**Word count:** 4064

## Abstract

Glioblastoma (GBM) is a highly invasive brain neoplasia with an elevated recurrence rate after surgical resection. The CyclinD1 (Ccnd1)/Cdk4–RB1 axis is frequently altered in GBM, leading to over-proliferation by RB1 deletion or by Ccnd1/Cdk4 over-activation. By not so well understood mechanisms, high levels of Ccnd1-Cdk4 also promote GBM cell invasion. The purpose of this work is to elucidate the *in vivo* role of the cytoplasmic Ccnd1-Cdk4 activity in the dissemination of GBM. We show that Ccnd1 activates invasion of primary human GBM cells through cytoplasmic RB1-independent mechanisms. By using GBM mouse models, we have observed that evaded GBM cells showed cytoplasmic Ccnd1 co-localizing with regulators of cell invasion such as RalA and Paxillin. Our genetic data strongly suggest that, in GBM cells, the Ccnd1/Cdk4 complex is acting upstream of those regulators. Accordingly, expression of Ccnd1 induces FAK, RalA and Rac1 activities. Finally, *in vivo* experiments demonstrated that the expression of a membrane-targeted Ccnd1 form expanded the GBM dissemination. We conclude that Ccnd1-Cdk4 activity promotes GBM dissemination through cytoplasmic and RB1-independent mechanisms. Therefore, the inhibition of Ccnd1-Cdk4 activity may be useful to hinder dissemination of recurrent GBM.


**Keywords**: Glioblastoma, Cyclin D1, Cytoplasm, Migration, Tumor dissemination

## Introduction

Diffuse gliomas are the most frequent tumors in adult brain and are characterized by an extensive infiltration in brain parenchyma [1]. Among them, Glioblastoma (GBM) is the most common and aggressive (grade IV) and shows a median survival of 15 months [2,3]. In recent years, to achieve a most accurate classification and to increase diagnostic and predictive outcomes, a broad experimental pursuit has been to elucidate genetic and epigenetic alterations involved in diffuse glioma etiology and development [4–10]. For instance, we now know that a recurrent point mutation (R132H) in the isocitrate dehydrogenase 1 gene (*IDH1*) is mostly associated to low grade diffuse gliomas and a better prognosis [4,9–11]. All these genomic researches have brought about a new classification of diffuse gliomas based on molecular fingerprints together with histological grading [12]. In this classification, GBMs are divided in IDH-wildtype and IDH-mutant. Most GBM cases (90%) are IDH-wildtype, predominate in elderly patients and have poor prognosis. The remaining GBMs are IDH-mutant, are less aggressive with better prognosis, predominate in younger patients and evolved from a low grade glioma (secondary GBMs). In addition to the IDH status, there are other markers associated with specific subsets of patients. For instance, p53, ATRX and H3K27M mutations as well as the CpG island methylator phenotype are also used as prognosis markers for GBM [8,10].

At present, regardless of the molecular characteristics, the standard treatment of patients with GBM includes surgical resection, radiotherapy and chemotherapy with temozolomide [13], an alkylating drug whose effects can be alleviated by DNA repair enzymes. A significant number of patients show

intrinsic resistance to temozolomide due to the expression of an alkyltransferase encoded by the MGMT gene [14]. When the MGMT promoter is unmethylated, the expression of this DNA repair gene confers resistance to alkylating agents. Alternatively, patients with methylated MGMT promoter are sensitive to temozolomide [15,16].

After the treatment, recurrences are most likely due to incomplete resections of the infiltrated tumor. GBMs show specific histological patterns of invasion formed by the interaction of the tumor cells with their immediate environment [17,18]. For instance, cell migration along white matter tracts or blood vessels (perivascular) is frequently observed in biopsies.

Cyclin-dependent kinases 4 and 6 (Cdk4/6) are part of one of the core pathways more frequently altered in GBM [5,8]. D-type cyclins (Ccnd) complexed with Cdk4/6 kinases phosphorylate and inhibit Retinoblastoma protein (RB1) in the nucleus, thus promoting cell cycle entry and proliferation [19]. The activity of Ccnd-Cdk4/6 complexes can be hindered by the Cdk-inhibitors p16 (CDKN2A), p15 (CDKN2B) and p18 (CDKN2C). The most frequent alterations leading to the activation of the Cdk4/6 pathway in GBM are co-deletions of CDKN2A and CDKN2B loci (56%), amplification of CDK4 locus (14%) and deletion of RB1 locus (7.9%) [8]. The detection and analysis of these mutations are relevant for prognosis. For instance, the presence of homozygous deletions in CDKN2A and B loci drastically reduces the overall survival of IDH-mutant gliomas irrespective of whether they are grade III astrocytic tumors or GBMs [20]. In xenograft models, GBM growth is significantly reduced after treatment with pharmacological inhibitors of Cdk4/6 activity [21,22]. However, RB1 non-expressing GBMs are resistant to this treatment [23,24].

The movement of invading cells along the extracellular matrix requires the coordination of different processes. Invading cells have to detach themselves partially from the matrix and, at the same time, to extend protrusions such as lamellipodia to undergo migration [25]. The knockdown (KD) of Ccnd1 in macrophages and fibroblasts stimulates a reduction in the levels of adhesion and spreading on fibronectin plates and, at the same time, increases cell migration and invasion capacities [26,27]. Also, Ccnd1 downregulation in GBM cell lines not only attenuates their proliferation but also their invasiveness [28,29]. Contrasting with the nuclear role of Ccnd1-Cdk4 in the regulation of proliferation, the control of cell invasiveness by Ccnd1-Cdk4 involves cytoplasmic mechanisms and targets [30,31]. In a previous work, we have described that cytoplasmic Ccnd1-Cdk4 promotes invasion in mouse fibroblasts and rat tumor cells through the phosphorylation of the focal adhesion component Paxillin (Pxn) and the Ral GTPase Exchange Factor (GEF) Rgl2 [30,32]. Ccnd1-Cdk4 induces the phosphorylation of Pxn at serine 83 [30], which is involved in Focal Adhesion Kinase (FAK) and Rac1 activation [33]. On the other hand, Rgl2 activation promotes accumulation of Ral-GTP [34].

The purpose of this work is to reveal the importance of cytoplasm-associated Ccnd1 activity in the invasive properties of primary human tumor cells. We show that cytoplasmic Ccnd1-Cdk4 plays a role in the dissemination of GBM *in vivo*.

## Materials and Methods

### Cell culture methods

GBM cell lines U251-MG and U87-MG were obtained from ATCC. Cell line authentication was carried out by comparing the STR profile with the reference

cell line in ATCC (Cell line authentication service, StabVida). Cells were maintained in DMEM media containing 10% FBS, penicillin/streptomycin at 37°C and 5% $CO_2$ atmosphere. Palbociclib (Selleckchem) was used at a final concentration of 2 μM or 5 μM. Primary GBM cell cultures were isolated as previously described [35]. We finally managed to establish 12 primary cultures, 10 GBM and 2 astrocytoma (grade II), and characterized Ccnd1, Cdk4, RB1 and IDH1 status in all of them. For further studies, we have used three strains with different RB1 and CDKN2A status: GBM65 (RB1-defective; CDKN2A-wildtype), GBM6 (RB1-wild type; CDKN2A-defective) and GBM55 (RB1-wildtype; CDKN2A-wildtype). Proliferation, viability, spreading and invasion assays were adapted from previously described protocols [30] and are detailed in Supplementary Methods. For experiments using Palbociclib, we treated the cells with the inhibitor for 12 h before the experiment.

**Expression vectors**

Human CCND1, mouse Pxn and human Rgl2 were used to obtain an N-terminal 3×HA fusion under UBI or CMV promoters in a lentiviral vector derived from pDSL (Invitrogen). Site-directed mutagenesis primers were used to obtain the different mutant alleles of the above genes as described in Supplementary Methods.

The dominant-negative allele RalBS28N was obtained from Addgene (CJ Der). Plasmid pMmCcnD1 was obtained from MRC (Image ID 3155470).

**Immunofluorescence (IF) and Immunohistochemistry (IHC)**

Cells were washed in PBS and fixed in 4% paraformaldehyde (PFA) for 15 min at RT. Fixed GBM cells were permeabilized with 0.2% Triton-X-100 for 3 min at RT, and blocked with 3% Bovine Serum Albumin (BSA). For tissue

immunofluorescence, fixed mouse brains were treated with 30% sucrose overnight, included in Tissue Freezing medium (EMS 72592) and kept at -80ºC. Slides of 20 μm were prepared in a cryostat and stored at -80ºC until use. Samples were transferred to RT and permeabilized with Methanol-Acetone at -20ºC. In both protocols, primary antibodies were combined with adequate Alexa488 and/or Alexa594-labelled secondary antibodies. Nuclei were stained with Hoescht. For GFP staining, we performed a sandwich with two secondary Alexa488 antibodies (goat anti-rabbit and rabbit anti-goat) to increase the signal. Images were acquired using 40X and 60X objectives in an Olympus FV1000 confocal system and EVOS microscope. Primary antibodies are described in supplementary material, Table S1.

Details of IHC in paraffin blocks can be found in Supplementary Methods. A Tissue MicroArray (TMA) containing 20 samples of GBM and 20 samples of Astrocytoma (TMA-324) was obtained from the Spanish National Cancer Research Center (CNIO) Biobank.

**Immunoblotting and Ral pull-down assay**

For immunoblot, protein samples were resolved by SDS-PAGE, transferred to PVDF membranes (Millipore), and incubated with primary antibodies (Table S1). Appropriate peroxidase (HRP)-linked secondary antibodies (GE Healthcare) were detected using the chemiluminescent HRP substrate Immobilon Western (Millipore). Chemiluminescence was recorded with a ChemiDoc-MP imaging system (BioRad). Ral activity was analyzed by measuring the GTP-bound form of Ral. The assays were performed by using RalBP1 agarose (Upstate, cat# 14-415) according to the manufacturer's instructions (see Supplementary Methods).

**Studies in humans and animals statement**

Human samples for primary cultures were provided by the Biobank of IRBLleida authorized by the Department of Health of Catalonia and registered in the National Register of Biobanks of the Carlos III Institute of Health with B.0000682 reference number. The study was conducted following the principles of the Declaration of Helsinki (World Medical Association, 1964) and with the approval of the Ethics Committee for Scientific Research (CEIC) of HUAV-UdL. Studies involving experiments with animals were subjected to approval by the Commission of Animal Experimentation (CEA), pursuant to Decree 214/1997 and Royal Decree 53/2013, from the Spanish law on the use of animals for experimentation and other scientific purposes. The experiments were performed in the animal facility of the University of Lleida (L-registration number 9900005).

**Mouse models**

Immunodeficient SCID hr/hr male mice (12-week-old; 20–25 g) were maintained in specific pathogen free conditions, and were injected with $5\times10^5$ U87 luciferase-expressing cells by intracranial injection in the subventricular zone of the right hemisphere (2 mm left to Bregma, 1 mm anterior to Coronal suture, 3 mm depth). Depending on the experiment, animals were euthanized 21 or 28 days after cell injection, brains were analyzed by bioluminescence and fluorescence, and finally fixed with PFA; a sample was included in paraffin for hematoxylin–eosin (H&E) staining and immunohistochemistry analysis. Luciferine was injected in the animals and the signal was recorded with a PhotonIMAGER and the software Photo-Acquisition. Image analysis was carried out in M3Vision™.

In the gliomagenesis model, tumors were generated by the injection of RCAS-hPDGFα viruses in neonatal mice (*Nestin/tv-a;Cdkn2a*$^{-/-}$). Samples were obtained from mice as previously described [36].

**Statistical analyses**

Two-tailed t-test allowing unequal variance or Mann-Whitney test were used (*P<0.05, **P<0.01, ns no significant). Comparisons among groups were made by one way ANOVA and Tukey-HSD post-test. Throughout the paper error bars indicate SEM except in Fig. 4E (mean ± SD). In Fig. 4D mean values and confidence limits for a proportion were calculated. Analyses of results obtained from mice are detailed in Supplementary Methods.

## Results

**RB1-independent functions of cyclin D1 regulate the invasion efficiency of GBM cells.**

To address the importance of the Ccnd1-Cdk4-RB1 regulatory pathway in human GBM, first we analyzed the expression levels of Ccnd1, Cdk4 and RB1 in primary GBM cells, grade II astrocytoma cells as well as in U251-MG and U87-MG GBM cell lines (Figure 1A). All the GBM samples showed expression of Ccnd1 and Cdk4, most displaying higher levels than the low-grade astrocytoma samples and GBM cell lines. In contrast, RB1 expression exhibited different levels among GBM samples and was not detected in two of these (GBM65 and GBM66). The Cdk4 specific inhibitor Palbociclib impinges upon the proliferation rate of GBM cells only when RB1 is present [22–24]. Hence, in order to confirm lack of RB1 expression in GBM65, we tested the growth rate of these cells after inhibition of Cdk4 activity with Palbociclib as compared to the

RB1-positive strain GBM6. As expected, Palbociclib abated the growth rate of the GBM6 strain (Figure 1B) but had no effect on the growth of GBM65 (Figure 1C).

The original tumors of GBM65 (RB1-negative) and two RB1-positive samples GBM55 and GBM6 were further characterized by IHC to determine the IDH1 and CDKN2A ($p16^{INKA}$) status. All these samples belonged to IDH1 wild type group of GBM (supplementary material, Figure S1). Regarding the CDKN2A status, positive staining for $p16^{INKA}$ was present in GBM65 and GBM55 but it was not observed in the GBM6 sample (supplementary material Figure S1). Then, GBM6 cells could support higher Ccnd1-Cdk4 activity than GBM55 and GBM65 due to the absence of this cell cycle inhibitor. Next, we also tested the MGMT-promoter methylation status of GBM6 and GBM65 samples (supplementary material, Figure S2A). In accordance with their methylation status, only GBM65 cells expressed MGMT and were consequently resistant to Temozolomide (supplementary material, Figure S2B and S2C).

Finally, to test the importance of Ccnd1-Cdk4 activity on GBM invasiveness, we determined the efficiency of invasion of RB1-negative (GBM65) and RB1-positive (GBM6 and GBM55) primary GBM cells. Interestingly, GBM cell invasion capacity was clearly reduced by Palbociclib regardless of RB1 status (Figure. 1D and supplementary material, Figure S3A and S3C), whereas cell viability was not affected by the treatment with the inhibitor (Figure. 1E and supplementary material, Figure S3B and S3D). Similarly, the knockdown of Ccnd1 reduced the invasion efficiency of both RB1-negative (GBM65) and RB1-positive (GBM6, U251-MG and U87-MG) cells (Figure. 1F and supplementary material Figure S3E-H), whereas it increased spreading on fibronectin plates

(Figure 1G and supplementary material Figure S3I and S3J). We conclude that Ccnd1-associated activity promotes cell invasion and reduces adhesion in primary GBM cells independently of RB1. Our data also suggest that Ccnd1-Cdk4 inhibition efficiently reduced invasiveness of GBM cells in different CDKN2A and MGMT-expression backgrounds.

**Localization of the Ccnd1-Cdk4 activity in GBM cells.**

By using patient derived glioma-tissue microarrays (TMA), we further confirmed that Ccnd1 expression is higher in GBM than in grade I and II astrocytoma biopsies (Figure 2A and 2B) [37,38]. However, only a small proportion of cells showed clear cytoplasmic signal for Ccnd1 (Figure 2C). This result was not completely unexpected as in other solid tumors Ccnd1 is preferentially accumulated in the cytoplasm of cells located at the invasive fronts [39]. Then, to better analyze Ccnd1 localization during GBM invasion, we have used a mouse model of gliomagenesis, which allows us to visualize the dissemination of tumor cells along the entire brain [36]. We infected neonatal *Nestin/tv-a Cdkn2*$^{-/-}$ mice with an RCAS retroviral vector expressing human PDGFα. At four months of age, these mice showed human-like proneural GBM (Figure 2D) [36]. We found a strong nuclear signal for Ccnd1 in these tumors, but interestingly we also detected GBM cells containing cytoplasmic Ccnd1 that were escaping outside the tumor (Figure 2E). These cells also showed positive PDGFα receptor (PDGFRα) staining, a marker of proneural-like tumor cells [36].

To characterize further the localization of Ccnd1 in the invasive GBM cells, we next used a xenograft model wherein human GBM cells (U87-MG) were injected into the brains of SCID mice. To determine the localization of Ccnd1,

U87-MG cells were infected with lentiviral particles harboring an HA-Ccnd1 construct (supplementary material, Figure S4B). Three weeks after the injection, mice developed intracranial tumors. We have observed that a high proportion of cells in the tumor mass showed HA-Ccnd1 accumulated in the nucleus (Figure 3A and 3C). In contrast, most of the evaded cells (such as perivascular cells) exhibited a sharp cytoplasmic signal for HA-Ccnd1 (Figure 3B and supplementary material, Figure S4A). Moreover, Ccnd1 also co-localized with cytoplasmic targets such as Pxn [30] and RalA [32] in the cytoplasm and membranes of primary GBM cells (Figure 3D and E and supplementary material, Figure S4C). These results reinforce the idea that cytoplasmic Ccnd1 could promote invasion of human GBM cells through the regulation of Pxn and Ral GTP activity.

**Ccnd1 promotes FAK, Rac1 and RalA activation in human GBM cells.**

To study the Ccnd1/Cdk4-Pxn-FAK-Rac1 axis in human GBM, first we determined the impact of Ccnd1 expression on FAK activation. Expression of Ccnd1 in GBM65 cells stimulated the phosphorylation of FAK at tyrosine 397 (Figure 4A and 4B), a key event in FAK activation.

Next, we analyzed the levels of Rac1 activation in GBM cells with YFP-PBD, a construct that is a fluorescent biosensor of Rac1 activity [40] because the p21-binding domain of PAK1 (PBD) specifically binds to Rac1-GTP forms. There were fewer cells with accumulation of YFP signal in the membrane or protrusion tips in the GBM sample knocked down for Ccnd1 (Figure 4C and 4D). This was indicative of lesser Rac1 activity associated to the membranes in the absence of Ccnd1.

Finally, we determined RalA activity in GBM cells in different Ccnd1-expression conditions. By pull-down assays, we have observed an increase of active Ral (Ral-GTP) in cells expressing high levels of Ccnd1 (Figure 4E). Overall, our data indicate that Ccnd1-associated activity promotes the induction of the Pxn-FAK-Rac1 and Ral pathways in primary GBM cells. These observations suggest that this axis may be implicated in the cytoplasmic functions of Ccnd1 in GBM cell invasion

**Ccnd1 promotes invasion in human GBM cells through the stimulation of Rac1, FAK and RalA activities.**

Next, we used genetic approaches to dissect the role of Pxn and Ral GTPases as mediators of Ccnd1 signaling in GBM cells. We first infected GBM65 cells either with an allele of Pxn (Pxn S83A S178A) that cannot be phosphorylated by Ccnd1-Cdk4 or with a dominant negative allele of RalA (RalAS31N) (Figure 5B). GBM cells expressing these mutant alleles were less invasive than wild-type cells, suggesting that active Pxn and Ral pathways are required for GBM invasion (Figure 5A). In a second experiment, we infected GBM65 cells with a phosphomimetic allele of Pxn (S83E S178E) or with an Rgl2-CAAX construct, a RalGTPase activator targeted to cell membranes (Figure 5D). Then, we tested the invasion capacity of these cells after inhibition of Ccnd1-Cdk4 activity with Palbociclib. In the presence of these hyperactive alleles, the inhibition of Ccnd1-dependent activity produced a much more modest reduction in the invasion capacity of these cells than in wild-type cells (Figure 5C). This result is consistent with Ccnd1-Cdk4 regulating invasion of GBM65 cells through Pxn and Ral pathways.

We also tested the dependence of GBM-cell adhesion on Ccnd1, Pxn and Ral activities. U251-MG cells stably expressing the interfering RNA against human Ccnd1 (depleted of human Ccnd1) were transfected with mouse Ccnd1-GFP and, either a non-phosphorylatable Pxn allele (S83A S178A) or a dominant negative allele of RalB (RalBS28N). Cells expressing Ccnd1-GFP required more time to spread on fibronectin. However, this delay was not observed in the presence of inactive alleles of Pxn or Ral GTPase (Figure 5E), which suggests that Ccdn1 also regulates the adhesion of GBM cells through Pxn and Ral pathways.

To envisage the clinical relevance of cytoplasmic Ccnd1-associated activity, we have analyzed the frequency of genetic alterations for the cytoplasmic targets of Ccnd1-Cdk4. We have used the TCGA dataset of diffuse gliomas (GBM-LGG) from the GlioVis platform to obtain the data [41]. Interestingly, we have observed that an increment in gene copy number of RAC1 and RALA genes was linked with IDH wild type ("high-grade") gliomas (supplementary material, Figures S5A and S5B). Consequently, the activation of cytoplasmic targets of Ccnd1-Cdk4, RAC1 and RALA, appears associated with glioma aggressiveness. In accordance with the relevance of Ccnd1-Ck4 activity in glioma aggressiveness [20], we have also observed that only an increment in CCND1 gene dosage reduced IDH mutant ("low-grade") glioma survival (supplementary material, Figure S5C).

**Accumulation of Ccnd1 in cell membranes promotes GBM dissemination *in vivo.***

In a previous work, we fused the farnesylation site of K-Ras protein (CAAX) to the C-terminus of Ccnd1, creating in this way a Ccnd1 that associates to cell

membranes and promotes Ral activation and cell invasion in prostate and endometrium tumor cell lines [39]. In this work, we have expressed Ccnd1-CAAX in GBM cells and observed that the treatment with Palbociclib drastically reduced the invasion capacity of those cells (supplementary material, Figure S3I). This result suggests that inhibiting cytoplasmic Ccnd1 would reverse the invasive phenotype in GBM cells.

To test whether membrane-associated Ccnd1 promotes GBM dissemination in vivo, luciferase-expressing U87-MG cells were co-infected with lentiviral vectors expressing GFP and either Ccnd1-CAAX or wild-type Ccnd1. Cells were intracranially injected, and four weeks later mice were euthanized. The localization and size of the tumors were analyzed by bioluminescence (Figure 6A). Tumors harboring Ccnd1-CAAX exhibited distant nodes from the original tumor (Figures 6B and 6C) and showed disseminated groups of tumor cells (cell foci) into the surrounding brain tissue (Figures 6F and 6G). Conversely, control tumors remained for the most part encapsulated (Figures 6H and 6I). By ki67 staining, we determined that the proliferative status of the induced tumors were not significantly different regardless of the Ccnd1 allele expressed (Figures 6D and 6E). To evaluate tumor dissemination, we defined three areas (proximal, intermediate and distal) around the tumor mass (supplementary material, Figures S6A and S6B). We calculated the number of cell foci in each area (supplementary material, Figure S6C). Only those tumors that showed intermediate and distal cell foci were considered disseminated tumors. By these criteria, the total number of dispersed tumors was significantly increased in Ccnd1-CAAX samples (Figure 6J). Furthermore, we confirmed that Ccnd1-CAAX was localized in the cell membrane of evaded tumor cells

(supplementary material, Figure S7). Overall, these results indicate that the accumulation of Ccnd1 in the membrane of GBM cells promotes GBM dissemination *in vivo*.

## Discussion

Cytoplasmic Ccnd1-Cdk4 plays a role in the dissemination of GBM *in vivo*. Taking advantage of xenograft and RCAS-Tva models, we find that Ccnd1 is cytoplasmic mainly in evaded GBM cells but not within the tumor masses, and that the imposed accumulation of Ccnd1 at the cell membranes significantly increases the number of evaded cells away from the tumor mass. The findings presented here are in line with a number of works showing that Ccnd1 functionally interacts with cytoplasmic targets involved in the regulation of cell adhesion and invasion such as Filamin A, Pacsin, Rgl2 and Paxillin [30– 32,42]. Also, cytoplasmic Ccnd1 has been found at the invasive fronts of solid tumors [39] and the invasive blastoid variant of mantle cell lymphoma [43], suggesting an important role of cytoplasmic Ccnd1 in tumor invasion. Moreover, the accumulation of Ccnd1 at the cell membranes increases the metastatic potential of endometrial tumor cells in a lung-metastasis mouse model [39].

These findings may have clinical implications. Upon Ccnd1-Cdk4 inhibition, we have observed similar reduction of invasiveness in IDH wild-type cells with different CDKN2A, MGMT-methylation and RB1 backgrounds, highlighting that inhibition of Cdk4/6-activity may be a useful approach to reduce dissemination in a broad spectrum of gliomas. Of note, since GBM cell invasion is RB1-independent, the capacity of invasion of GBM cells is still sensitive to a Palbociclib treatment in the absence of RB1. This is in accordance with previous findings showing that the regulation of cell motility and invasion by

Ccnd1 in mouse fibroblasts is also RB1-independent [27]. In our xenograft experiments most tumors expressing membrane-associated Ccnd1 show GBM dissemination; yet, their proliferation ratio is similar to tumors expressing wild-type Ccnd1, emphasizing that the regulation of GBM cell invasion by Ccnd1 is unconnected to the proliferative status.

Our genetic data also indicate that Pxn is a downstream target of Ccnd1-Cdk4 in human GBM cells. Interestingly, Pxn seems to behave as an oncogene in glioma progression and its overexpression is associated with high-grade gliomas [44]. Also, a positive correlation among GBM invasiveness and Pxn phosphorylation at tyrosine 118 has been reported [45]. Here, we contribute with genetic approaches to demonstrate that phosphorylation of Pxn at S83 and S178 is required for efficient invasion and inefficient spreading of GBM cells. Conceivably, these phosphorylations triggered by Ccnd1 expression could constitute an initial step in the induction of GBM invasion. While specific phosphoPxn S83 (S85 in humans) and S178 antibodies for human cells are not available, we have observed that expression of Ccnd1 activates downstream targets of Pxn such as FAK and Rac1. Of note, the importance of these downstream targets in GBM invasion has also been reported by different authors [1,46,47]. For instance, in GBM cell lines, loss of FAK inhibits EGF-induced invasion [48], whereas Rac1 hyperactivation correlates with an elevated invasive phenotype [49,50].

Furthermore, the expression of a RalA dominant-negative allele reduced the invasion efficiency of primary GBM cells. Ral GTPases are regulators of exocyst formation and the secretory pathway, and are involved in the control of cell growth and invasion [34]. Furthermore, Ral activation also contributes to Ras-

driven transformation, and it is increased in many different types of cancer [51]. Surprisingly, very few data exist about the importance of Ral GTPases in GBM. Our results are consistent with a previous report showing that the knockdown of RalB decreases the invasiveness of human GBM cell lines [52].

We propose a model in which the cytoplasmic accumulation of Ccnd1-Cdk4 activity causes cell evasion in GBM through the activation of the Pxn-Fak-Rac1 axis and Ral GTPases (Figure 6K). Interestingly, cytoplasmic Ccnd1 has also been detected in human GBM recurrences after surgery and therapy [53]. Because Palbociclib inhibits both the nuclear and the cytoplasmic activities of Ccnd1-Cdk4, we propose that it does not only hinder cell proliferation in the presence of RB1, but also interferes with tumor dissemination independently of RB1 by precluding the cytoplasmic Ccnd1-Cdk4 activity. Then, it is conceivable to use the pharmacological inactivation of Ccnd1-Cdk4 as treatment not only against tumor cell proliferation but also against their invasive capacity. While additional work is required to address specifically the relevance of the cytoplasmic functions of Ccnd1-Cdk4 in glioma classification and outcome predictions, altogether, our results are in agreement with those works that sustain a clinical relevance of D-type cyclins and Cdk4/6 in the diagnosis and therapy of glioma [10,20].



**Acknowledgements**

We thank Sònia Rius, Marta Rafel, Laura Colàs, Ana Velasco and María Ruiz (IRBLleida-Biobank) for technical assistance, and María Jesús Artiga and Patricia González from Biobank and Histopathology Core Unit, CNIO for technical support. We specially thank Massimo Squatrito for providing the

samples of the gliomagenesis model. This work was funded by the Spanish Ministry of Education and Science (BFU2013-42895-P; BFU2016-78826-P) and the Instituto de Salud Carlos III/FEDER (P13/01980), and supported by the Xarxa de Bancs de Tumors de Catalunya sponsored by Pla Director d'Oncología de Catalunya (XBTC)", IRBLleida Biobank (B.0000682) and PLATAFORMA BIOBANCOS PT17/0015/0027". T. Cemeli (FPU13/06590) and I. Felip (FPU14/02674) were supported by a predoctoral fellowship from Ministerio de Educación, Cultura y Deportes and from Diputació de Lleida. M. Guasch and M. Nager were supported by a predoctoral fellowship from UdL. A.J. Schuhmacher was supported by a research contract from "Ramón y Cajal" program (RYC-2015-17622) by the Spanish Ministry for the Economy, Industry and Competitiveness (MINECO).

**Authors' contributions.** T.C. performed constructions and experiments. T.C., I.F., S.C., and M.G. performed mice xenograft experiments. M.N. and J.H. obtained primary GBM cultures. A.J.S. implemented the mouse gliomagenesis model and provided samples. M.S. and S.G. performed IHC and analyzed pathology data. M.N., F.F., X.D., J.H., S.C. A.J.S and N.P. provided cell-culture support, contributed materials and helped with procedures. E.G. designed the project and wrote the manuscript. All authors contributed discussions and comments on the manuscript.

## Abbreviations

**GBM**: Glioblastoma; **CcnD**: D type Cyclins; **Ccnd1**: Cyclin D1; **CDK4**: Cyclin-dependent kinase 4; **Pxn**: Paxillin; **RB**: Retinoblastoma; **FAK**: Focal Adhesion

Kinase; **PBD**: P21 Bindin Domain of PAK1; **Fluc**: Firefly Luciferase Gene; **GFP**: Green Fluorescent Protein; **YFP**: Yellow Fluorescent Protein; **WT**: Wildtype; **DMEM**: Dulbecco's modified Eagle's Medium; **FBS**: Fetal Bovine Serum; **PFA**: Paraformaldehyde; **BSA**: Bovine Serum Albumin; **PBS**: Phosphate Buffered Saline; **TMA**: Tissue MicroArray; **PVDF**: PolyViniliDene Fluoride; **HRP**: Horseradish peroxidase; **EDTA**: Ethylene diaminetetraacetic acid; **GTP**: Guanine TriPhosphate; **DTT**: Dithiothreitol; **SCID**: Severe Combined ImmunoDeficiency; **H&E**: Hematoxylin & Eosin; **IHC**: ImmunoHistoChemistry; **PDGFα**: Platelet Derived Growth Factor Alpha; **PDGFRα**: Platelet Derived Growth Factor Receptor Alpha; **SEM**: Standard Error of the Mean.

## Supplementary Information

- Supplementary data with suppl. figure legends and suppl. data of methods (including antibodies, primers and statistics)
- Supplementary figure 1
- Supplementary figure 2
- Supplementary figure 3
- Supplementary figure 4
- Supplementary figure 5
- Supplementary figure 6
- Supplementary figure 7

## References

1 Louis DN. MOLECULAR PATHOLOGY OF MALIGNANT GLIOMAS. *Annu Rev Pathol Mech Dis* 2006; **1**: 97-117

2 Alifieris C, Trafalis DT. Glioblastoma multiforme: Pathogenesis and treatment. *Pharmacol Ther* 2015; **152**: 63-82

3 Schwartzbaum JA, Fisher JL, Aldape KD, *et al.* Epidemiology and molecular pathology of glioma. *Nat Clin Pract Neurol* 2006; **2**: 494-503

4 Parsons DW, Jones S, Zhang X, *et al.* An integrated genomic analysis of human glioblastoma multiforme. *Science (80- )* 2008; **321**: 1807-1812

5 Cancer Genome Atlas Research Network. Comprehensive genomic characterization defines human glioblastoma genes and core pathways. *Nature* 2008; **455**: 1061-1068

6 Verhaak RGW, Hoadley KA, Purdom E, *et al.* Integrated Genomic Analysis Identifies Clinically Relevant Subtypes of Glioblastoma Characterized by Abnormalities in PDGFRA, IDH1, EGFR, and NF1. *Cancer Cell* 2010; **17**: 98-110

7 Noushmehr H, Weisenberger DJ, Diefes K, *et al.* Identification of a CpG Island Methylator Phenotype that Defines a Distinct Subgroup of Glioma. *Cancer Cell* 2010; **17**: 510-522

8 Brennan CW, Verhaak RGW, McKenna A, *et al.* The somatic genomic landscape of glioblastoma. *Cell* 2013; **155**: 462-477

9 Cancer Genome Atlas Research Network. The Cancer Genome Atlas Research Network. Comprehensive, Integrative Genomic Analysis of Diffuse Lower-Grade Gliomas. *N Engl J Med* 2015; **372**: 2481-2498

10 Ceccarelli M, Barthel FP, Malta TM, *et al.* Molecular Profiling Reveals

Biologically Discrete Subsets and Pathways of Progression in Diffuse Glioma. *Cell* 2016; **164**: 550-563

11 Balss J, Meyer J, Mueller W, *et al.* Analysis of the IDH1 codon 132 mutation in brain tumors. *Acta Neuropathol* 2008; **116**: 597-602

12 Louis DN, Perry A, Reifenberger G, *et al.* The 2016 World Health Organization Classification of Tumors of the Central Nervous System: a summary. *Acta Neuropathol* 2016; **131**: 803-820

13 Stupp R, Hegi ME, Mason WP, *et al.* Effects of radiotherapy with concomitant and adjuvant temozolomide versus radiotherapy alone on survival in glioblastoma in a randomised phase III study: 5-year analysis of the EORTC-NCIC trial. *Lancet Oncol* 2009; **10**: 459-466

14 Esteller M, Garcia-Foncillas J, Andion E, *et al.* Inactivation of the DNA-Repair Gene MGMT and the Clinical Response of Gliomas to Alkylating Agents. *N Engl J Med* 2000; **343**: 1350-1354

15 Hegi ME, Diserens AC, Godard S, *et al.* Clinical Trial Substantiates the Predictive Value of O-6-Methylguanine-DNA Methyltransferase Promoter Methylation in Glioblastoma Patients Treated with Temozolomide. *Clin Cancer Res* 2004; **10**: 1871-1874

16 Paz MF, Yaya-Tur R, Rojas-Marcos I, *et al.* CpG island hypermethylation of the DNA repair enzyme methyltransferase predicts response to temozolomide in primary gliomas. *Clin Cancer Res* 2004; **10**: 4933-4938

17 Cuddapah VA, Robel S, Watkins S, *et al.* A neurocentric perspective on glioma invasion. *Nat Rev Neurosci* 2014; **15**: 455-465

18 Scherer HJ. Structural development in gliomas. *Am J Cancer* 1938; **34**: 333-351

19 Sherr CJ, Roberts JM. CDK inhibitors: positive and negative regulators of G1-phase progression. *Genes Dev* 1999; **13**: 1501-1512

20 Shirahata M, Ono T, Stichel D, *et al.* Novel, improved grading system(s) for IDH-mutant astrocytic gliomas. *Acta Neuropathologica*. 2018:1-14.

21 Fry DW, Harvey PJ, Keller PR, *et al.* Specific inhibition of cyclin-dependent kinase 4/6 by PD 0332991 and associated antitumor activity in human tumor xenografts. *Mol Cancer Ther* 2004; **3**: 1427-1438

22 Michaud K, Solomon DA, Oermann E, *et al.* Pharmacologic inhibition of cyclin-dependent kinases 4 and 6 arrests the growth of glioblastoma multiforme intracranial xenografts. *Cancer Res* 2010; **70**: 3228-3238

23 Wiedemeyer WR, Dunn IF, Quayle SN, *et al.* Pattern of retinoblastoma pathway inactivation dictates response to CDK4/6 inhibition in GBM. *Proc Natl Acad Sci* 2010; **107**: 11501-11506

24 Cen L, Carlson BL, Schroeder MA, *et al.* P16-Cdk4-Rb axis controls sensitivity to a cyclin-dependent kinase inhibitor PD0332991 in glioblastoma xenograft cells. *Neuro Oncol* 2012; **14**: 870-881

25 Gardel ML, Schneider IC, Aratyn-Schaus, Y, *et al.* Mechanical Integration of Actin and Adhesion Dynamics in Cell Migration. *Annu Rev Cell Dev Biol* 2010; **26**: 315-333

26 Neumeister P, Pixley FJ, Xiong Y, *et al.* Cyclin D1 governs adhesion and

motility of macrophages. *Mol Biol Cell* 2003; **14**: 2005-2015

27 Li Z, Wang C, Jiao X, *et al.* Cyclin D1 regulates cellular migration through the inhibition of thrombospondin 1 and ROCK signaling. *Mol Cell Biol* 2006; **26**: 4240-4256

28 Arato-Ohshima T, Sawa H. Over-expression of cyclin D1 induces glioma invasion by increasing matrix metalloproteinase activity and cell motility. *Int J Cancer* 1999; **83**: 387-392

29 Wang J, Wang Q, Cui Y, *et al.* Knockdown of cyclin D1 inhibits proliferation, induces apoptosis, and attenuates the invasive capacity of human glioblastoma cells. *J Neurooncol* 2012; **106**: 473-484

30 Fusté NP, Fernández-Hernández R, Cemeli T, Mirantes C, Pedraza N, Rafel M, Torres-Rosell J, Colomina N, Ferrezuelo F, Dolcet X GE. Cytoplasmic cyclin D1 regulates cell invasion and metastasis through the phosphorylation of paxillin. *Nat Commun* 2016; **7**: 11581

31 Zhong Z, Yeow W-S, Zou C, *et al.* Cyclin D1/cyclin-dependent kinase 4 interacts with filamin A and affects the migration and invasion potential of breast cancer cells. *Cancer Res* 2010; **70**: 2105-2114

32 Fernández RMH, Ruiz-Miró M, Dolcet X, *et al.* Cyclin D1 interacts and collaborates with Ral GTPases enhancing cell detachment and motility. *Oncogene* 2011; **30**: 1936-1946

33 Ishibe S, Joly D, Liu Z-X, *et al.* Paxillin serves as an ERK-regulated scaffold for coordinating FAK and Rac activation in epithelial morphogenesis. *Mol Cell* 2004; **16**: 257-267

34 Bodemann BO, White MA. Ral GTPases and cancer: Linchpin support of the tumorigenic platform. *Nat Rev Cancer* 2008; **8**: 133-140

35 Nàger M, Sallán MC, Visa A, Pushparaj C, Santacana M, Macià A, Yeramian A, Cantí C HJ. Inhibition of WNT-CTNNB1 signaling upregulates SQSTM1 and sensitizes glioblastoma cells to autophagy blockers. *Autophagy* 2018; **14**: 619-636

36 Ozawa T, Riester M, Cheng YK, *et al.* Most human non-GCIMP glioblastoma subtypes evolve from a common proneural-like precursor glioma. *Cancer Cell* 2014; **26**: 288-300

37 Martínez-Sáez E, Peg V, Ortega-Aznar A, *et al.* peIF4E as an independent prognostic factor and a potential therapeutic target in diffuse infiltrating astrocytomas. *Cancer Med* 2016; **5**: 2501-2512

38 Chakrabarty A, Bridges LR, Gray S. Cyclin D1 in astrocytic tumours: An immunohistochemical study. *Neuropathol Appl Neurobiol* 1996; **22**: 311-316

39 Fusté NP, Castelblanco E, Felip I, Santacana M, Fernández-Hernández R, Gatius S, Pedraza N, Pallarés J, Cemeli T, Valls J, Tarres M, Ferrezuelo F, Dolcet X, Matias-Guiu X GE. Characterization of cytoplasmic cyclin D1 as a marker of invasiveness in cancer. *Oncotarget* 2016; **7**: 26979-26991

40 Hoppe AD, Swanson JA. Cdc42, Rac1 and Rac2 Display Distinct Patterns of Activation during Phagocytosis. *Mol Biol Cell* 2004; **15**: 1895-1903

41 Bowman RL, Wang Q, Carro A, *et al.* GlioVis data portal for visualization

and analysis of brain tumor expression datasets. *Neuro Oncol* 2017; **19**: 139-141

42 Meng H, Tian L, Zhou J, *et al.* PACSIN 2 represses cellular migration through direct association with cyclin D1 but not its alternate splice form cyclin D1b. *Cell Cycle* 2011; **10**: 73-81

43 Body S, Esteve-Arenys A, Miloudi H, *et al.* Cytoplasmic cyclin D1 controls the migration and invasiveness of mantle lymphoma cells. *Sci Rep* 2017; **7**: 13946

44 Sun LH, Yang FQ, Zhang CB, *et al.* Overexpression of Paxillin Correlates with Tumor Progression and Predicts Poor Survival in Glioblastoma. *CNS Neurosci Ther* 2017; **23**: 69-75

45 Arscott WT, Tandle AT, Zhao S, *et al.* Ionizing Radiation and Glioblastoma Exosomes: Implications in Tumor Biology and Cell Migration. *Transl Oncol* 2013; **6**: 638-648

46 Riemenschneider MJ, Mueller W, Betensky RA, *et al.* In situ analysis of integrin and growth factor receptor signaling pathways in human glioblastomas suggests overlapping relationships with focal adhesion kinase activation. *Am J Pathol* 2005; **167**: 1379-1387

47 Salhia B, Tran NL, Symons M, *et al.* Molecular pathways triggering glioma cell invasion. *Expert Rev Mol Diagn* 2006; **6**: 613-626

48 Jones G, Machado J, Merlo A. Loss of focal adhesion kinase (FAK) inhibits epidermal growth factor receptor-dependent migration and induces aggregation of NH2-terminal FAK in the nuclei of apoptotic

glioblastoma cells. *Cancer Res* 2001; **61**: 4978-4981

49 Okura H, Golbourn BJ, Shahzad U, *et al.* A role for activated Cdc42 in glioblastoma multiforme invasion. *Oncotarget* 2016; **7**: 1-18

50 Salhia B, Rutten F, Nakada M, *et al.* Inhibition of Rho-kinase affects astrocytoma morphology, motility, and invasion through activation of Rac1. *Cancer Res* 2005; **65**: 8792-8800

51 Gentry LR, Martin TD, Reiner DJ, *et al.* Ral small GTPase signaling and oncogenesis: More than just 15 minutes of fame. *Biochim Biophys Acta - Mol Cell Res* 2014; **1843**: 2976-2988

52 Song X, Hua L, Xu Y, *et al.* Involvement of RalB in the effect of geranylgeranyltransferase I on glioma cell migration and invasion. *Clin Transl Oncol* 2015; **17**: 477-485

53 Pirtoli L, Belmonte G, Toscano M, *et al.* Cyclin D1 co-localizes with beclin-1 in glioblastoma recurrences: A clue to a therapy-induced, autophagy-mediated degradative mechanism? *Anticancer Res* 2016; **36**: 4057-4062



## Figure legends

**Figure 1.** *Ccnd1 regulates the efficiency of cell invasion and adhesion independently of RB1*. **A)** Immunoblot to detect Ccnd1, Cdk4 and RB1 in primary GBMs, low grade gliomas and, U251-MG and U87-MG GBM cell lines. Actin staining was used as loading control. **B and C)** Respectively, the same number of RB1-positive (GBM6) and RB1-negative (GBM65) cells were treated

with the Ccnd1-Cdk4 inhibitor Palbociclib (5 μM) (time 0) and total cell number was determined after 36 and 72 hours (n=3). **D)** RB1-negative GBM65 cells were incubated in the presence of Palbociclib (5 μM) in a transwell device coated with matrigel. After 8 hours of incubation, invading cells were counted (n=3). **E)** Viable and total cells in D were counted (n=3). The ratio of viable (trypan-blue negative) to total cells is drawn. **F)** GBM65 cells were infected with scramble (scr) or shRNA anti-Ccnd1 (shD1) and the invasion efficiency tested as in D (n=5). The lower panel shows the levels of Ccnd1 and actin as a loading control. **G)** RB1-negative GBM65 cells infected with scramble (scr) or shRNA anti-Ccnd1 (shD1) were seeded on fibronectin plates, incubated for 30 minutes, and both spread and total cells were counted (n=3). For all the experiments, data are the mean ± SEM, and statistical significance was determined by student-t test. *($p \leq 0.05$) ** ($p \leq 0.01$) ns = not significant.

**Figure 2**. *Expression and localization of Ccnd1 in GBMs*. **A)** Representative Ccnd1 staining of Glioma samples from the Tissue MicroArray (TMA). **B)** Boxplot representing the proportion of Ccnd1-positive cells from samples of low-grade astrocytoma and GBM. Significance was determined by Mann–Whitney U test ($p=0.022$). **C)** Representative image of GBM cells expressing cytoplasmic Ccnd1. Arrows indicate cells with cytoplasmic localization. **D and E)** Images from immunohistochemical analyses with the indicated antibodies and H&E from a selected region of a RCAS hPDGFα-driven tumor. The images correspond to consecutive slices. Boxes show an enlarged region. Scale bars, 100 μm.

**Figure 3.** *Ccnd1 localizes in the cytoplasm of GBM cells and co-localizes with Pxn and RalA.* **A)** U87-MG cells infected with lentiviral particles containing a 3HA-Ccnd1 were injected into the brains of SCID mice to initiate intracranial tumors. Three weeks after injection, brains were cryopreserved and processed for IF. Anti-HA (green) and anti-Glut1 (red) antibodies were used for the detection of HA-Ccnd1 and blood vessels, respectively. Images were acquired by confocal microscopy (10 μm bar). Nuclei were stained with Hoescht (blue). The white contour designates regions with tumor cells. **B)** Representative image of evaded cells in A. **C)** From three independent mouse brains, we counted the number of infected cells (green) showing nuclear accumulation of HA-Ccnd1. Data are the mean ± SEM, and statistical significance (n=3) was determined by student-t test (** p≤0.01). **D** and **E)** Cells were seeded on fibronectin plates for two hours, then fixed in 4% PFA and permeabilized with 0.2% Triton X-100. Images were acquired by confocal microscopy (10 μm bar). Nuclei were stained with Hoescht (blue). Antibodies were: Anti-Ccnd1 (green), anti-Pxn (red) in D and anti-RalA (red) in E.

**Figure 4.** *Ccnd1 stimulates Fak, Rac1 and RalA activation in human GBM cells.* **A)** Ccnd1-knockdown GBM65 cells (shD1) were transfected with mouse Ccnd1 (MmD1, n=9) or GFP (n=6). Cells were maintained in low serum for 16 hours before collecting samples. FAK Y397, β-Actin and Ccnd1 were determined by immunoblot. **B)** The levels of protein were determined by densitometry with the Image-Lab 4.0.1 software from Bio-Rad. β-Actin was used as a loading control. Data are expressed as mean ± SEM. Significance was determined by a t-test. **C)** GBM65 cells were infected with interference RNA against Ccnd1 or with a

scrambled RNA as a control. Once Ccnd1 was downregulated, cells were transfected with the YFP-PBD construct (a sensor of Rac1 activity). Two days after transfection, cells were seeded on fibronectin for 2 h prior fixation and processing (10 μm bar). Arrows indicate membrane regions with accumulation of YFP. **D)** The experiment in C was independently repeated twice. Mean values and confidence limits ($\alpha$=0.05; n≥100) are plotted. **E)** Ccnd1-knockdown GBM65 cells (shD1) were transfected with mouse Ccnd1 (MmD1) or GFP. Twenty-four hours later, active RalA-GTP was affinity purified with RalBP-beads from cell lysates. RalA-GTP and total RalA were detected by immunoblotting. RalBP-beads are shown as pull-down control. The experiment was repeated twice. Relative mean values ± SD for the RalA-GTP/total RalA ratios are shown.

**Figure 5.** *Ccnd1 promotes invasion of human GBM cells through Paxillin phosphorylation and Ral activation.* **A)** GBM65 cells were infected with wild-type Pxn, a non-phosphorylatable Pxn allele or the dominant negative allele RalAS31N. Forty eight hours later, cells were seeded on 24-well transwell filters previously coated with matrigel, and allowed to invade for seven hours. Values are expressed as mean ± SEM (n=3). Significance was determined by one way ANOVA and Tukey-HSD post-test (*p<0.05). **B)** Immunoblots showing the expression of Pxn and Ral alleles (rat anti-HA) in the infected cells in A. Actin was used as a loading control. **C)** GBM65 cells were infected with a phosphomimetic Pxn allele or with Rgl2-CAAX. The invasion efficiency was tested as in A but cells were also treated with Palbociclib (5 μM), or DMSO as a control. **D)** Immunoblots showing the expression of Pxn and Ral alleles (rat anti-HA) in the infected cells in C. Actin was used as a loading control. **E)** U251 cells

stably expressing shD1 were transfected with GFP as a control (vector) or with Ccnd1-GFP, and then co-transfected with the non-phosphorylatable Pxn allele (S83A S178A) or with the dominant negative allele RalBS28N. Percentage of spreading was determined as in Figure 1G. Values are expressed as mean ± SEM (n=3). Significance was determined by one way ANOVA and Tukey-HSD post-test (**p<0.01).

**Figure 6.** *Membrane-targeted Ccnd1 induces GBM dissemination* in vivo. Human U87-MG cells stably expressing luciferase were co-infected with lentiviruses harboring GFP and Ccnd1-CAAX, Ccnd1, or an empty vector (control). Infected cells were inoculated intracranially in immunodeficient SCID male mice. For the experiment, we have finally used in total 27 mice, nine for each condition. Mice were euthanized four weeks after intracranial injection with these infected cells. Brains were processed for cryopreservation. To detect tumor cells (green), serial slides of the brain were immunostained with a rabbit anti-GFP antibody conjugated with Alexa Fluor-488 (from Invitrogen). The mouse brain (red) was contrasted with a secondary anti-mouse Alexa Fluor-594 antibody (from Invitrogen). **A)** Tumor location and size was observed by luciferine-mediated luminescence. **B)** Representative image of a tumor expressing Ccnd1-CAAX showing disseminated nodules (arrows). **C)** Luminescence and GFP pictures showing a contralateral nodule in sample 2.2. **D)** Representative pictures of Ki67 staining immunosatining. **E)** Percentage of Ki67-positive cells (mean ± SEM, n=5 for each condition). **F** and **G)** Images from a tumor expressing Ccnd1-CAAX showing evaded tumor cells (arrow). **H** and **I)** Images from an encapsulated-control tumor. **J)** Plot showing the number

of disseminated versus non disseminated tumors (n=9 for each condition). The statistical significance was calculated with a Fisher's exact test (*p<0.05; **p<0.01). **K)** A diagram of the proposed Ccnd1-Cdk4 regulatory network in GBM cells.

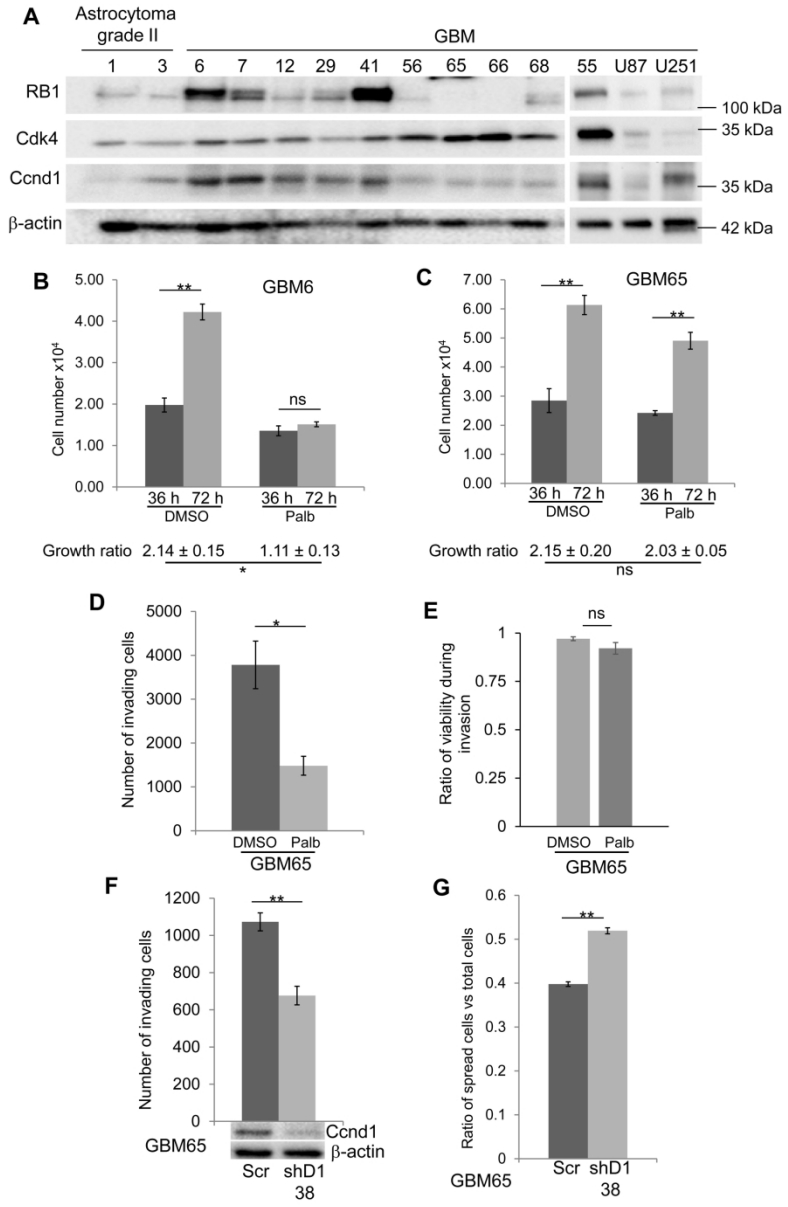


Figure 1

166x257mm (300 x 300 DPI)

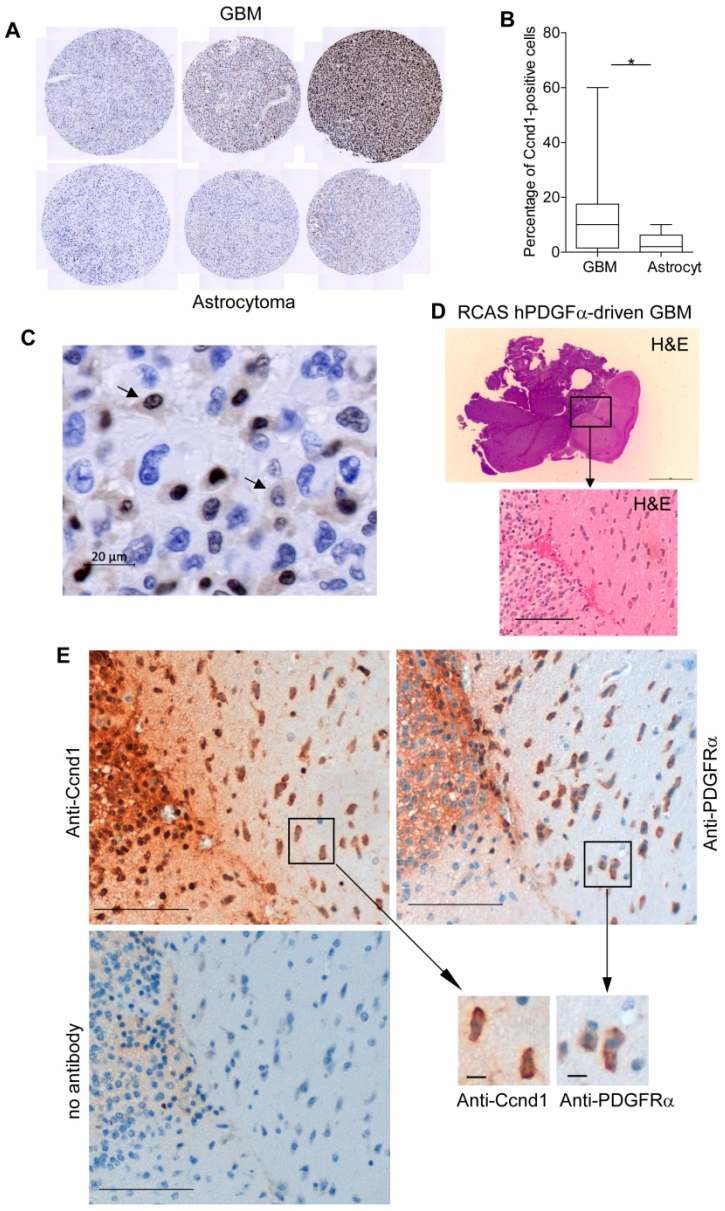
A
GBM
Astrocytoma
B
Percentage of Ccnd1-positive cells
80
60
40
20
0
*
GBM
Astrocyt
C
20 µm
D
RCAS hPDGFα-driven GBM
H&E
H&E
E
Anti-Ccnd1
Anti-PDGFRα
no antibody
Anti-Ccnd1
Anti-PDGFRα

Figure 2

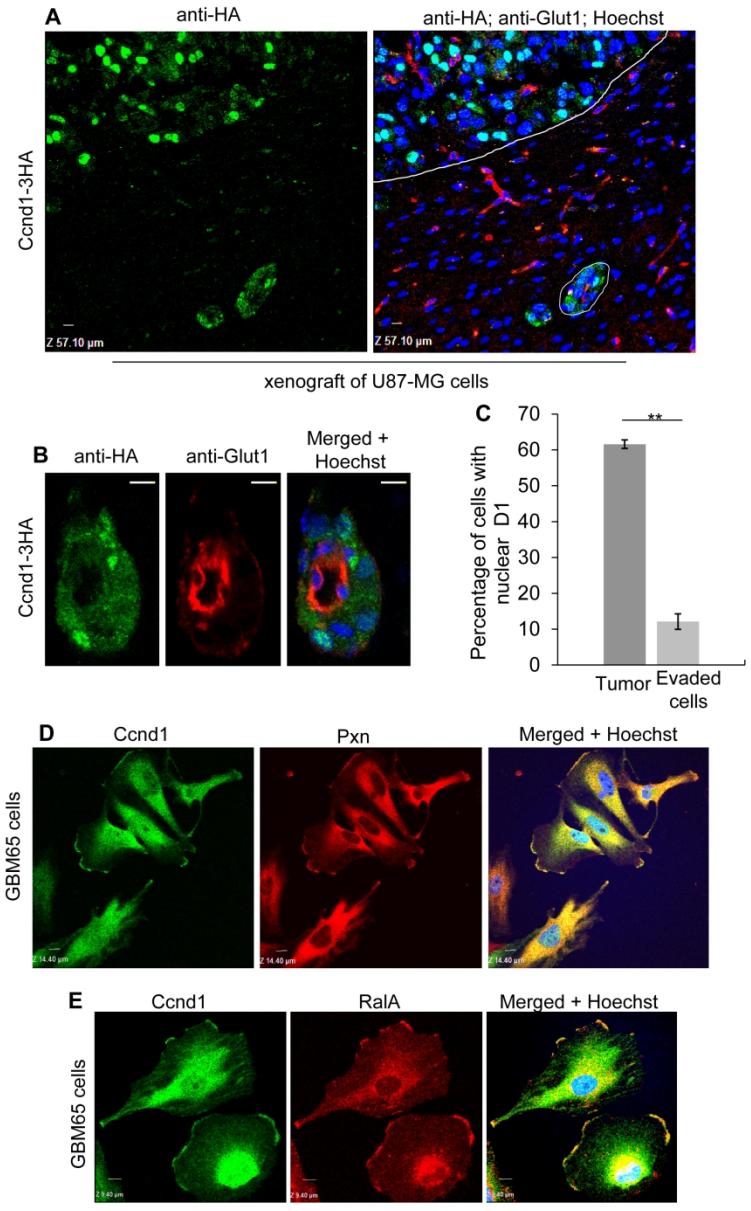
A
anti-HA
anti-HA; anti-Glut1; Hoechst
Ccnd1-3HA
Z 57.10 µm
Z 57.10 µm
xenograft of U87-MG cells
B
anti-HA
anti-Glut1
Merged + Hoechst
Ccnd1-3HA
C
Percentage of cells with nuclear D1
70
60
50
40
30
20
10
0
**
Tumor
Evaded cells
D
Ccnd1
Pxn
Merged + Hoechst
GBM65 cells
E
Ccnd1
RalA
Merged + Hoechst
GBM65 cells

Figure 3

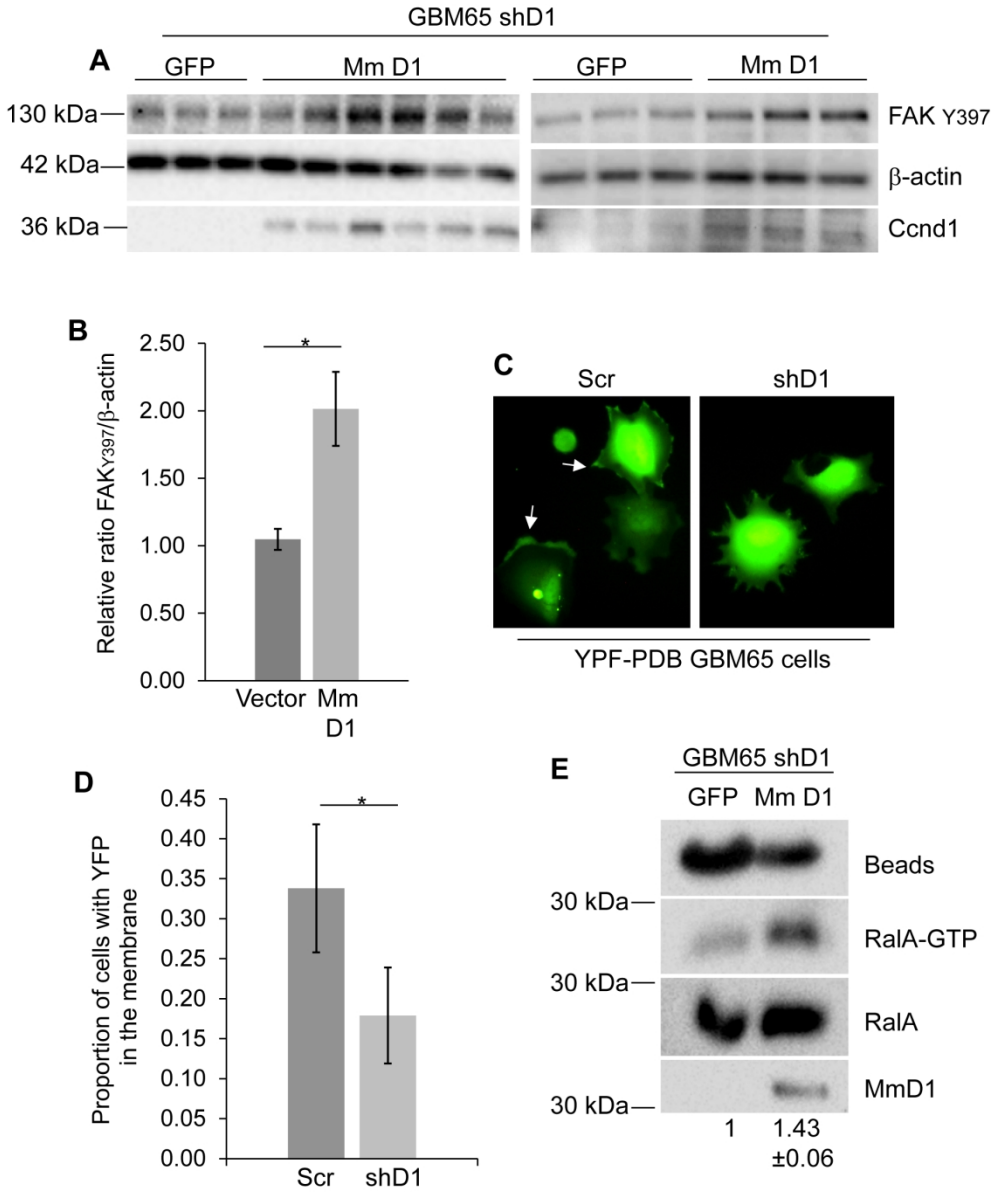
GBM65 shD1
A
GFP
Mm D1
GFP
Mm D1
130 kDa
42 kDa
36 kDa
FAK Y397
β-actin
Ccnd1
B
Relative ratio FAKY397/β-actin
2.50
2.00
1.50
1.00
0.50
0.00
*
Vector
Mm D1
C
Scr
shD1
YPF-PDB GBM65 cells
D
Proportion of cells with YFP in the membrane
0.45
0.40
0.35
0.30
0.25
0.20
0.15
0.10
0.05
0.00
*
Scr
shD1
E
GBM65 shD1
GFP
Mm D1
Beads
30 kDa
RalA-GTP
30 kDa
RalA
MmD1
30 kDa
1
1.43
±0.06

Figure 4

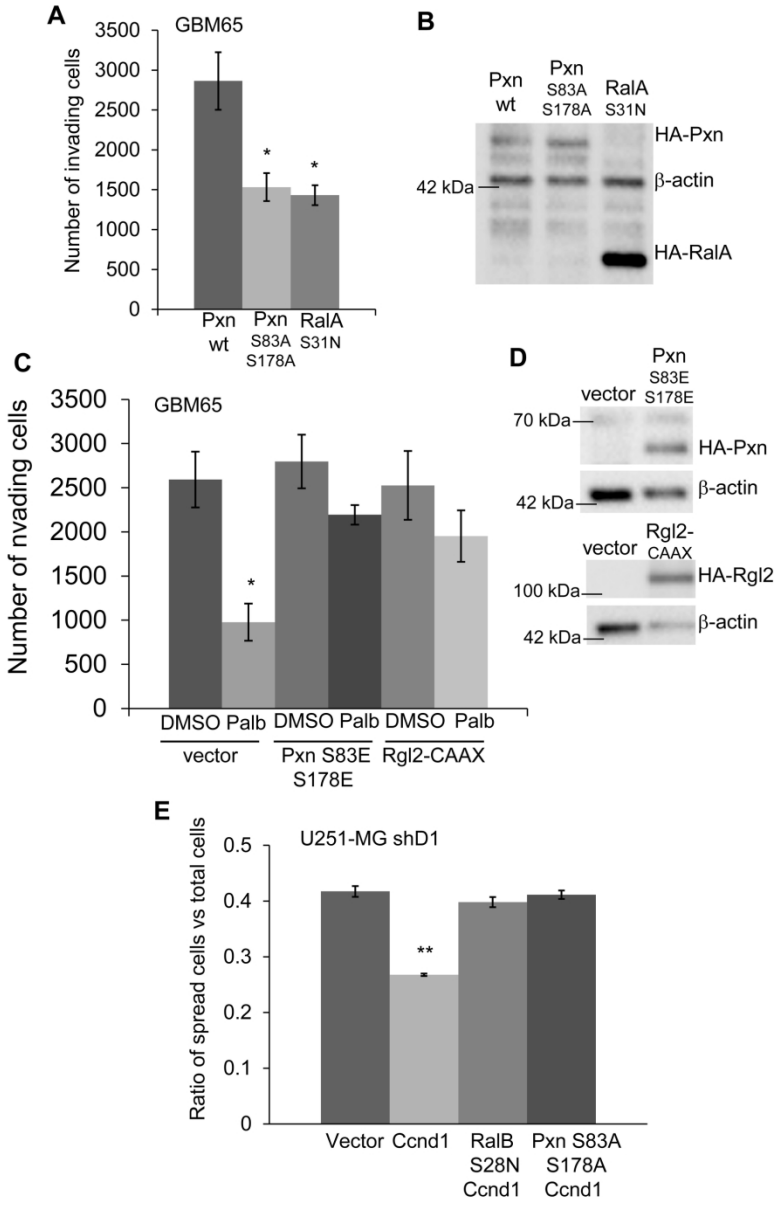


Figure 5

152x231mm (300 x 300 DPI)

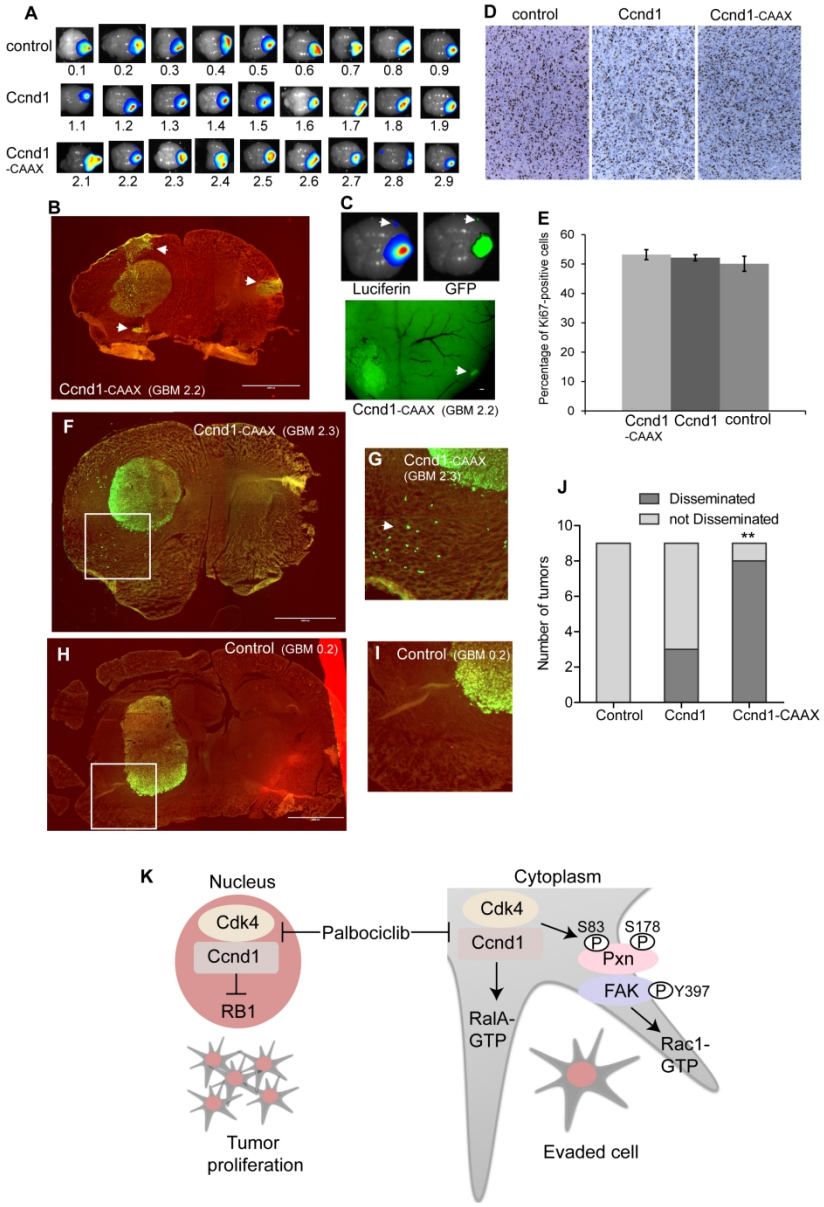
A
control
Ccnd1
Ccnd1 -CAAX
0.1 0.2 0.3 0.4 0.5 0.6 0.7 0.8 0.9
1.1 1.2 1.3 1.4 1.5 1.6 1.7 1.8 1.9
2.1 2.2 2.3 2.4 2.5 2.6 2.7 2.8 2.9
D
control
Ccnd1
Ccnd1-CAAX
B
Ccnd1-CAAX (GBM 2.2)
C
Luciferin
GFP
Ccnd1-CAAX (GBM 2.2)
E
Percentage of Ki67-positive cells
Ccnd1 -CAAX
Ccnd1
control
F
Ccnd1-CAAX (GBM 2.3)
G
Ccnd1-CAAX (GBM 2.3)
J
Disseminated
not Disseminated
Number of tumors
Control
Ccnd1
Ccnd1-CAAX
H
Control (GBM 0.2)
I
Control (GBM 0.2)
K
Nucleus
Cdk4
Ccnd1
RB1
Palbociclib
Cytoplasm
Cdk4
Ccnd1
S83
S178
Pxn
FAK
Y397
RalA-GTP
Rac1-GTP
Tumor proliferation
Evaded cell

Figure 6

**Supplementary Figure 1.** *IDH1 and CDKN2A status.* Slides of the original tumors of GBM6, GBM55 and GBM65 were processed for IHC analyses. IDH1 status was tested with a mouse monoclonal antibody against the IDH1 R132H point mutation (DIA-H09, Dianova). A positive IDH1 mutant specimen was used as a positive control. CDKN2A status was tested with a mouse monoclonal antibody against $p16^{INKa}$ (E6H4, Roche).

**Supplementary Figure 2.** *MGMT promoter methylation status.* A) The methylation status of the MGMT promoter was resolved in primary GBM samples and cell lines by pyrosequencing after bisulfite treatment. B) The expression of MGMT was determined in GMB6 and GBM65 cells by immunoblot. β-actin was used as a loading control. C) The primary GBM cells were treated with the alkylating drug Temozolomide 100 μM (TMZ) and cell growth was determined by MTT staining after ten days of treatment (n=4). Data are the mean ± SEM, and statistical significance was determined by one-ANOVA test (*** p≤0.001).

**Supplementary Figure 3.** *Ccnd1-Cdk4 activity regulates the efficiency of cell invasion in GBM cells*. **A** and **C).** GBM cells were incubated in the presence of Palbociclib (2μM) in a transwell device coated with matrigel at 37ºC and 5% $CO_2$. After eight hours of incubation, invading cells were counted (n=3) **B** and **D).** Cells in A and C were incubated with Palbociclib (2μM) for eight hours, and after this time, viable and total cells were counted (n=3). The ratio of viable (trypan-blue negative) cells versus total cells is drawn. **E)** U251-MG cells were infected with scramble (scr) or with two different shRNA anti-Ccnd1 ($shD1_{38}$ and $shD1_{39}$) and the invasion efficiency tested as in A (n=4). **F)** The downregulation of Ccnd1 in E

was tested by immunoblot. Actin was used as a loading control. **G** and **H)** U87-MG and GBM6 cells were respectively infected with scramble (scr) or with the shRNA anti-Ccnd1 shD1$_{38}$ and the invasion efficiency tested as in A (n=3). **I)** GBM65 cells were infected with Ccnd1-CAAX and incubated in a transwell device coated with matrigel at 37ºC and 5% $CO_2$. Palbociclib (5μM) was added. After eight hours of incubation, invading cells were counted (n=3). **J** and **K)** U251-MG and U87-MG cells were infected with shD1$_{38}$ or with a scramble shRNA as a control. To test spreading, cells were seeded in serum-free medium in fibronectin-coated plates. Thirty minutes later the proportion of spread cells was determined and plotted (n=4). For all the experiments, data are the mean ± SEM and statistical significance was determined by student-t test. *($p \leq 0.05$) ** ($p \leq 0.01$). ns = not significant.

**Supplementary Figure 4.** *Ccnd1 co-localizes with Pxn and RalA in the cytoplasm and membranes of GBM cells.* **A)** U87-MG cells infected with 3HA-Ccnd1 were injected into the brains of SCID mice. Three weeks after injection, samples were processed for IF. The antibodies used were anti-HA (green) and anti-Glut1 (red) for the detection of blood vessels (red). Images were acquired by confocal microscopy (10μm bar). Nuclei were stained with Hoescht (blue). **B)** The topical expression of Ccnd1 in A was tested by immunoblot with anti-Ccnd1. Actin was used as a loading control. **C)** Cells were seeded in fibronectin plates for 24 hours, then fixed in 4% PFA and permeabilized with 0.2% Triton X-100. Images were acquired by confocal microscopy (10μm bar). Nuclei were stained with Hoescht (blue). The antibodies used were Anti-Ccnd1 (green), anti-Pxn and anti-

RalA (red). **D**) Cells incubated only in the presence of secondary antibodies were used as a control.

**Supplementary Figure 5.** *Relevance of cytoplasmic Ccnd1-associated activity in gliomas outcome.* **A)** and **B)** Analysis of the genetic status of RAC1 (A) and RALA (B) genes from a TCGA cohort of diffuse gliomas (Gliovis). The percentages of the different alterations in IDH wild-type and mutant gliomas were plotted. **C)** From the same population than in A, we selected a subset of IDH mutant gliomas that were wild-type diploids for CDK4/6, CCND1/2/3, RAC1, RALA and CDKN2A/B (CDKN2A/B wt; n=176). Then, we have analyzed survival times (months) with a Kaplan-Meier plot comparing the effects of a copy number increase of CCND1 (gain; n=14) and homozygous deletion of CDKN2A/B (homodel; n=14). Hetloss, heterozygous loss; Diploid, wild type alleles; and Amp, amplification.

**Supplementary Figure 6.** *Quantification of GBM dissemination* in vivo. **A** and **B)** we have defined three areas (P-proximal, I-intermediate and D-distal) around the tumor mass to estimate the extent of tumor dissemination. **C)** Plot showing the number of cells foci at different areas outside the tumor mass. Data are the mean ± SEM (n=9 for each condition). The statistical significance was calculated with a Kruskal-Wallis test (* $p<0.05$).

**Supplementary Figure 7.** *Ccnd1-CAAX localizes in the membrane of human U87-MG cells in intracranial induced tumors.* Human U87-MG cells were infected with lentiviruses harboring HA-Ccnd1-CAAX **(A)** or HA-Ccnd1 **(B)**. These cells

were inoculated by intracranial injection in nude SCID mice, and three weeks later mice were sacrificed. Brains were obtained and included in paraffin for IHC detection. H&E staining was used to visualize the induced tumor. Ccnd1 localization was detected with a rat monoclonal anti-HA and nuclei were stained with hematoxylin.

## Supplementary Table S1

| Antibody | Reference | IHC[1] | IF[2] | IB[3] |
|---|---|---|---|---|
| **Anti-Ccnd1** | Rabbit monoclonal clone EP12, Dako #M3642 | Ready to use | 1/200[5] | - |
| **Anti-Ccnd1** | Mouse monoclonal DCS-6, BD Pharmigen #556470 | - | - | 1/500 |
| **Anti-Pxn** | Mouse monoclonal 349, BD Biosciences #610051 | - | 1/200 | - |
| **Anti-RalA** | Mouse monoclonal 8, BD Pharmigen #610222 | - | 1/200 | 1/2000 |
| **Anti-HA** | Rat monoclonal clone 3F10, Roche 11867423001 | 1/400 | 1/200[5] | - |
| **Anti-Glut1** | Mouse monoclonal SPM498, Thermofisher #MA-11315 | - | 1/200[5] | - |
| **Anti-GFP** | Rabbit polyclonal, Invitrogen A21311 | - | 1/200[5] | - |
| **Anti-Ki67** | Clone MIB-1, Agilent tecnhonogies-DAKO. | Ready to use | - | - |
| **Anti-phosphoFAK (Tyr 397)** | Rabbit polyclonal, Clone 31H5L17, Thermofisher #700255 | 1/100 | - | 1/500[4] |
| **Anti-Cdk4** | Rabbit polyclonal C-22, SantaCruz #sc-260 | - | - | 1/250 |
| **Anti-RB** | Mouse monoclonal G3-245, BD Pharmigen #554136 | - | - | 1/500 |
| **Anti-Actin** | Mouse monoclonal Clone C4, Millipore #MAB1501R | - | - | 1/1000 |
| **Anti-Rac1** | Mouse monoclonal 102, BD Pharmigen #610222 | - | - | 1/2000 |
| **Anti-IDH1 R132H** | Mouse monoclonal H09, Dianova DIAH09 | Ready to use | - | - |
| **Anti-p16I$^{NKa}$** | Mouse monoclonal E6H4, Roche CINtec® Histology Kit | Ready to use | - | - |
| **Anti-MGMT** | Mouse monoclonal MT3.1, Millipore MAB16200 | - | - | 1/1000 |

1- IHC: Immunohistochemistry
2- IF: Immunofluorescence
3- IB: Immunoblot
All antibodies were used in BSA 0,3% except the ones marked 4 (BSA 3%) and 5 (BSA 4% + 0.04 Tween-20)

## Supplementary Methods

### Transfection and lentiviruses production

Transient transfection of vectors was performed with Lipofectamine 2000 (Invitrogen) according to manufacturer's instructions.

For lentivirus production, HEK293T cells were transfected with lentiviral expression vectors, envelope plasmid pVSV.G, and packaging plasmid pHR'82ΔR at a ratio 2:1:1. Stable expression of Luciferase was carried out by lentiviral infection of U87-MG cells and selection in 6 μg/ ml of Hygromycin.

For RNA interference the CCND1 MISSION shRNAs TRCN0000026838 and TRCN0000026839 cloned in a pLKO.1-puro were obtained from Sigma.

The YFP-PBD vector was obtained from J. Swanson via Addgene.

### Expression vectors. Site-directed mutagenesis.

Standard PCR-mediated site-directed mutagenesis was used to obtain the different mutant alleles of Ccnd1, Rgl2 and Pxn. The 3' end of the K-Ras ORF containing the CAAX motif (GGC TGT GTG AAA ATT AAA AAA TGC ATT ATA ATG TAA; aa179–189) was fused to the 3' end of the CCND1 and RGL2 human ORFs. To obtain the non-phosphorylatable and phosphomimetic mutants of mouse Paxillin (IMAGE ID 5309957 clone from Source BioScience) were used the following primers:

GCGCCACTGCCCGTGTACAGCTC/CGGAGGCTGCTGGTGAGCGT for S83A;

GCGCCCCTTTATGGCATCCCAGA/CAGGGCTCCAGGCAAGGGGGG for S178A;

CCGGTGTACAGCTCCAGTGCTAA/TAGTGGCTCCGGAGGCTGCTGGTGAGCGT for S83E;

GAGCCCCTTTATGGCATCCCAGA/GAGGGCTCCAGGCAAGGGG for S178E.

Firefly luciferase gene (Fluc) was cloned under the control of the UBI promoter in the pLKO.1 hygromycin lentivirus.

**Immunohistochemistry (IHC)**

Paraffin blocks of human tumor tissue and mouse tissue samples were sectioned at a thickness of 3μm, dried for 1 hour at 65°C before de-parafinization, rehydration, and epitope retrieval in the Pre-Treatment Module, PT LINK (Dako, Glostrup, Denmark) at 95°C for 20 minutes in 50mM Tris/EDTA buffer, pH 9. Before staining the sections, endogenous peroxidase was blocked. *Samples were* visualized with the EnVision FLEX Detection Kit (Dako, Glostrup, Denmark) using diaminobenzidine chromogen as a substrate. Slides were counterstained with hematoxylin. Negative controls were obtained without the addition of the primary antibody. Primary antibodies are described in Supplementary Table 1.

**Ral pull-down assay**

Cell lysates were obtained from one 100mm plate of transfected GBM cells. The lysis buffer used was 50mM Tris pH 7.5, 200mM NaCl, 2.5mM $MgCl_2$, 2.5mM DTT, 1% Triton and protease and phosphatase inhibitors. An aliquot of 0.6ml of cell lysate was incubated with 10μg of RalBP1 beads for 30 min at 4°C and, after several washes, agarose beads were resuspended in 2x Laemmli buffer. Samples were separated by SDS-PAGE, transferred to PVDF membranes, and immunoblotted.

**Cell culture methods**

For proliferation assay, 15000 cells/well were seeded on a 24-well plate in triplicates. After 36 or 72 hours of treatment, cells were trypsinized and counted in a Neubauer's chamber. For cell viability determination, 0.2% Trypan Blue was added before counting.

Proliferation and viability were also determined with MTT assay. Cells were incubated at 37 °C 5% $CO_2$ during 1 hour with MTT at 1 mg/ml in darkness. Then, media was removed and DMSO was added into the wells to dissolve formazan crystals produced by living cells. Absorbance was read at 595 nm wavelength.

To measure cell spreading, petri dishes were coated overnight at 4 °C with a 5 µg /ml solution of fibronectin (Invitrogen) in PBS. Forty-eight hours after infection/transfection, cells were trypsinized and seeded in serum-free medium in the fibronectin-coated 35-mm well plates. Cells were incubated for one hour, fixed with 2% PFA, and spread cells were counted (n≥150 green cells were evaluated in each independent experiment). Round and bright cells were considered unspread.

We performed cell invasion assays with infected GBM cells. Briefly, 6.5-mm filters of 8.0 pore size (Transwell, Corning) were coated with Matrigel (full factor, BD Biosciences) in the bottom side. Then, infected cells (1-2×$10^4$) were seeded in the upper side of the filter. Afterwards, filters were loaded with DMEM 10% serum and incubated in 24-well plates containing serum-free medium for eight hours. Under these conditions, some cells migrate from the upper to the bottom side of the filter invading the Matrigel. The remaining cells at the upper side of the filter were removed, and Matrigel-embedded cells were fixed and stained with

Hoescht. We have counted all cells in the filter extension with the Image J software.

**Statistical analyses**

For mice studies (Fig. 6 and Supplementary Fig. S6), we have used the Ene 3.0: a program to calculate sample size. This software was developed by the Department of Applied Statistics of Autonomous University of Barcelona and is distributed by GlaxoSmithKline. No specific method of randomization was used but the group allocation was done randomly.

For the experiment in Figure 3, we inoculated four animals with U87-MG cells infected with Ccnd1-HA (two animals were inoculated with PBS as background controls). For the experiment in Figure 6, groups of 11-12 animals were inoculated with U87-MG-luciferase-GFP cells, U87-MG-luciferase-GFP-Ccnd1-HA cells or U87-MG-luciferase-GFP-Ccnd1-CAAX-HA cells. Some animals died during anesthesia and others were also discarded by the misleading location of the tumor. In those animals, the inoculated cells were scattered through the meninges and the tumor developed extra-cranially. Finally, we have analyzed three animals in figure 3 (n=3) and nine animals for each condition in figure 6 and supplementary figure 6 (n=27).

We have analyzed the differences in number of tumor-evaded cells by Kruskal-Wallis non-parametric test and Dunn's multiple comparison post-test. To assess the significance in the differences in the number of disseminated tumors, we have performed a Fisher's exact test.

**MGMT methylation**

The DNA of the samples were obtained from GBM cell cultures and subjected to a bisulfite treatment (MethylCode ™ Bisulfite Conversion Kit, MECOV50 ThermoFisher) prior to amplification by PCR. A single fragment covering a part of the promoter region is amplified and the degree of methylation is analyzed by a pyrosequencing reaction (MGMT Pyro Kit, ID: 970061 Qiagen).

**TCGA data analyses**

To analyze the clinical relevance of our model, we have obtained diagnosis, grading, survival and gene status data of 669 patients with diffuse gliomas from The Cancer Genome Atlas Project (TCGA-GBMLGG) using the GlioVis platform (http://gliovis.bioinfo.cnio.es/). For different genes codifying downstream targets of cytoplasmic Ccnd1, we have determined the percentage of amplifications (Amp), copy number increase (Gain), heterozygous loss (Hetloss) and homozygous deletions (Homdel) in two different groups, IDH1 wild type and mutant samples.

By using the same glioma source, we have designed a study to confirm the relevance of Ccnd1-Cdk4 activity in glioma prognosis. First, we have chosen as standard population a subset of 173 IDH-mutant samples all of them wild type diploids for CCND1/2/3, CDK4/6, CDKN2A/B, RAC1 and RALA. Then, we have selected other samples with the same background only changing either CCND1 copy number gain (n=14) or CDKN2A/B homozygous deletion (n=14). Both, CCND1 gain and CDKN2A/B homozygous deletion should stimulate Cdk4/6 activity. Overall survival in those three conditions was analyzed by the Kaplan–Meier method and compared with a log- rank test.

**Figure S1**

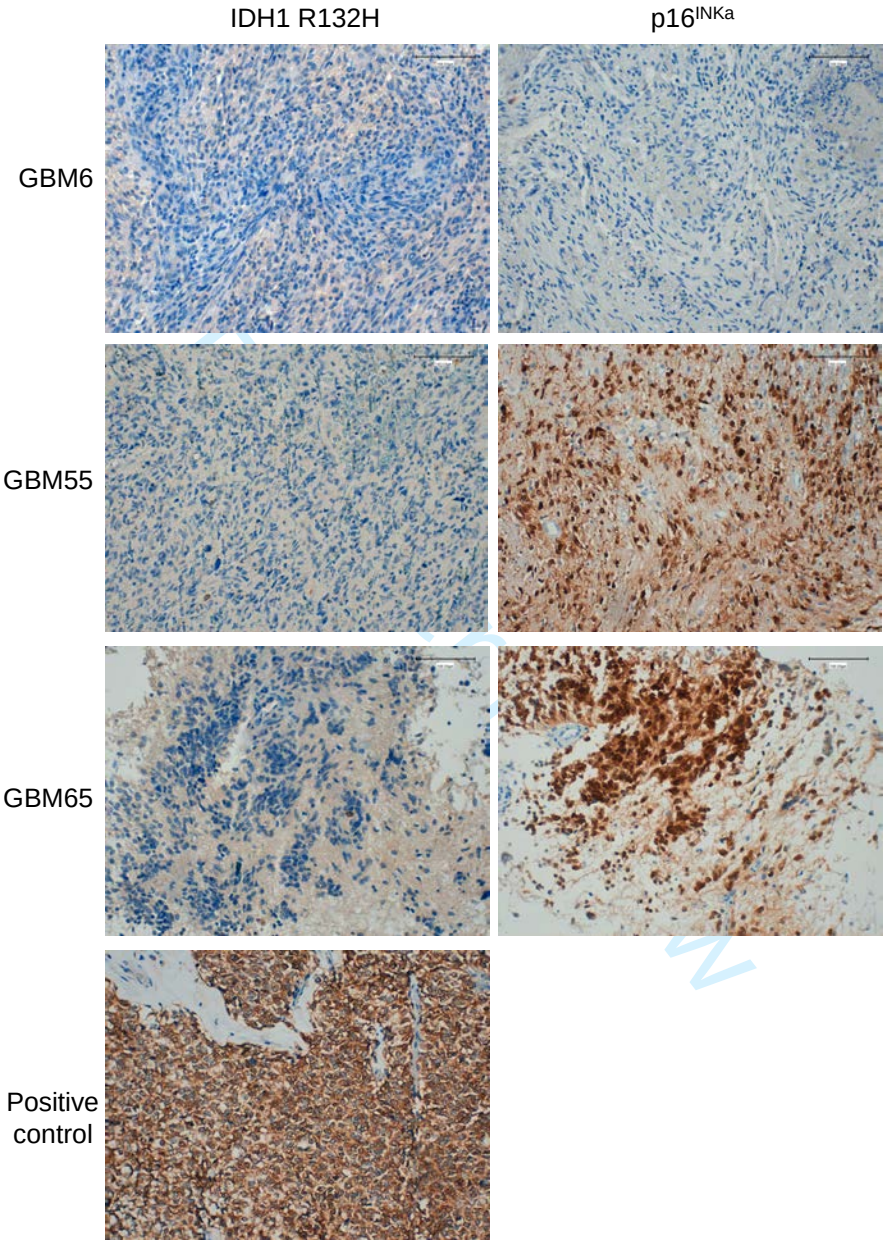

**Figure S2**

A

| Sample | MGMT-promoter status | Percentage of methylation |
|---|---|---|
| U251-MG | Methylated | 45 |
| U87-MG | Methylated | 74 |
| GBM6 | Methylated | 50 |
| GBM65 | Un-methylated | 1.5 |

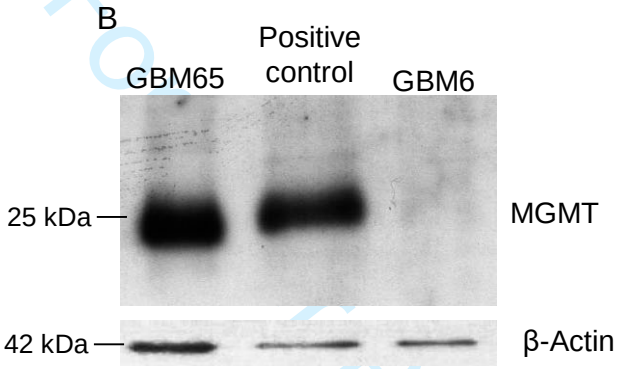


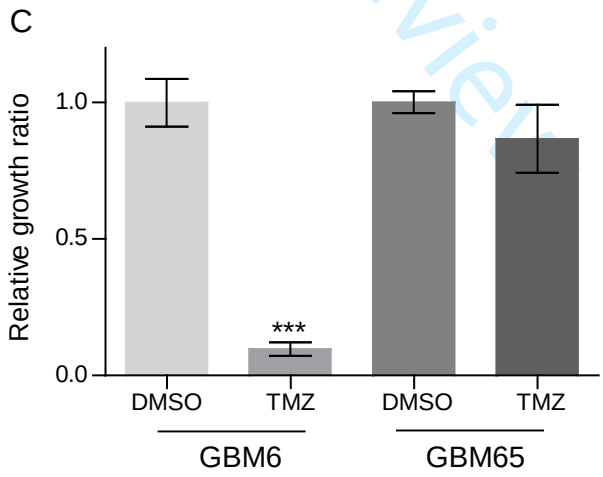

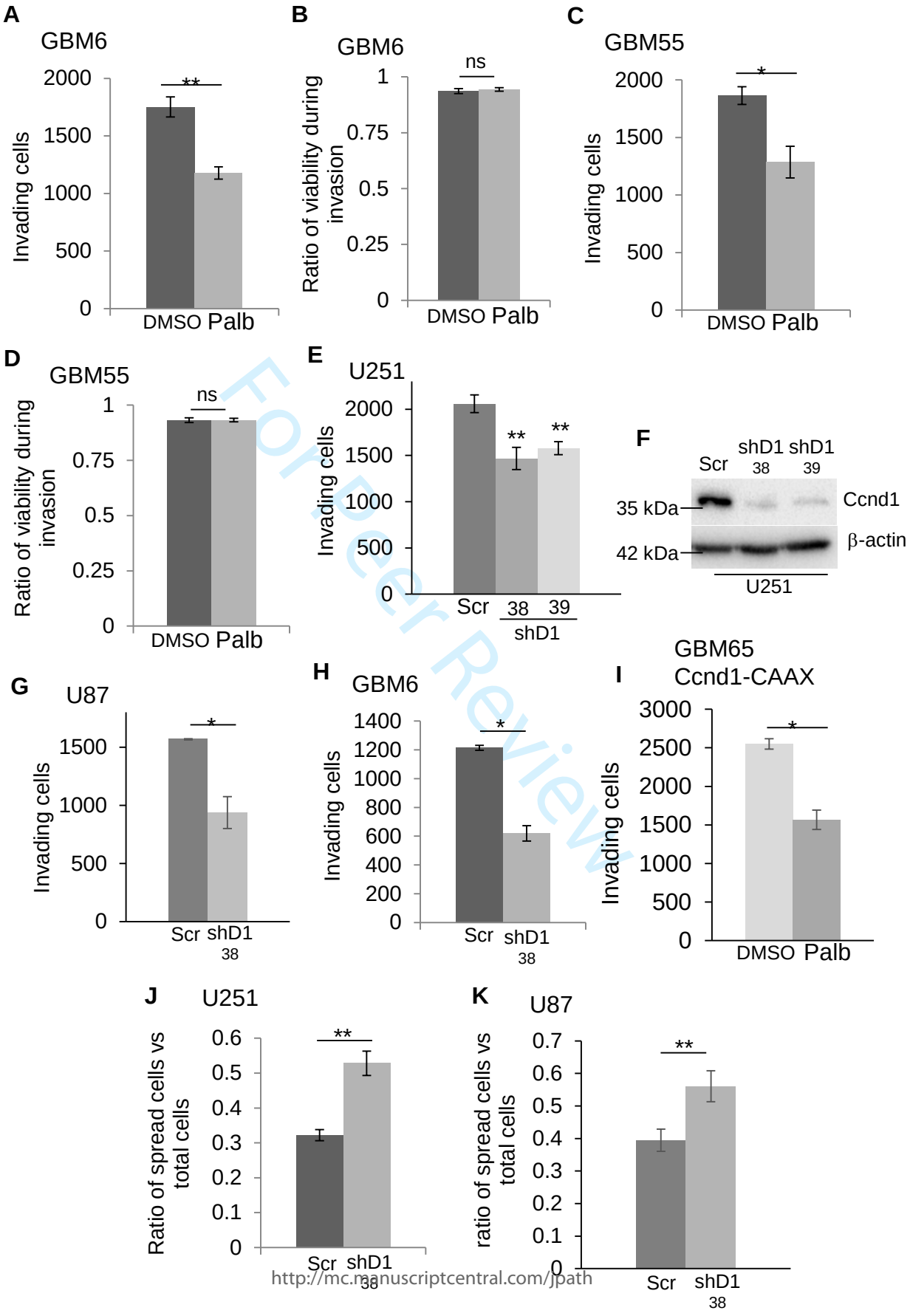

**Figure S4**

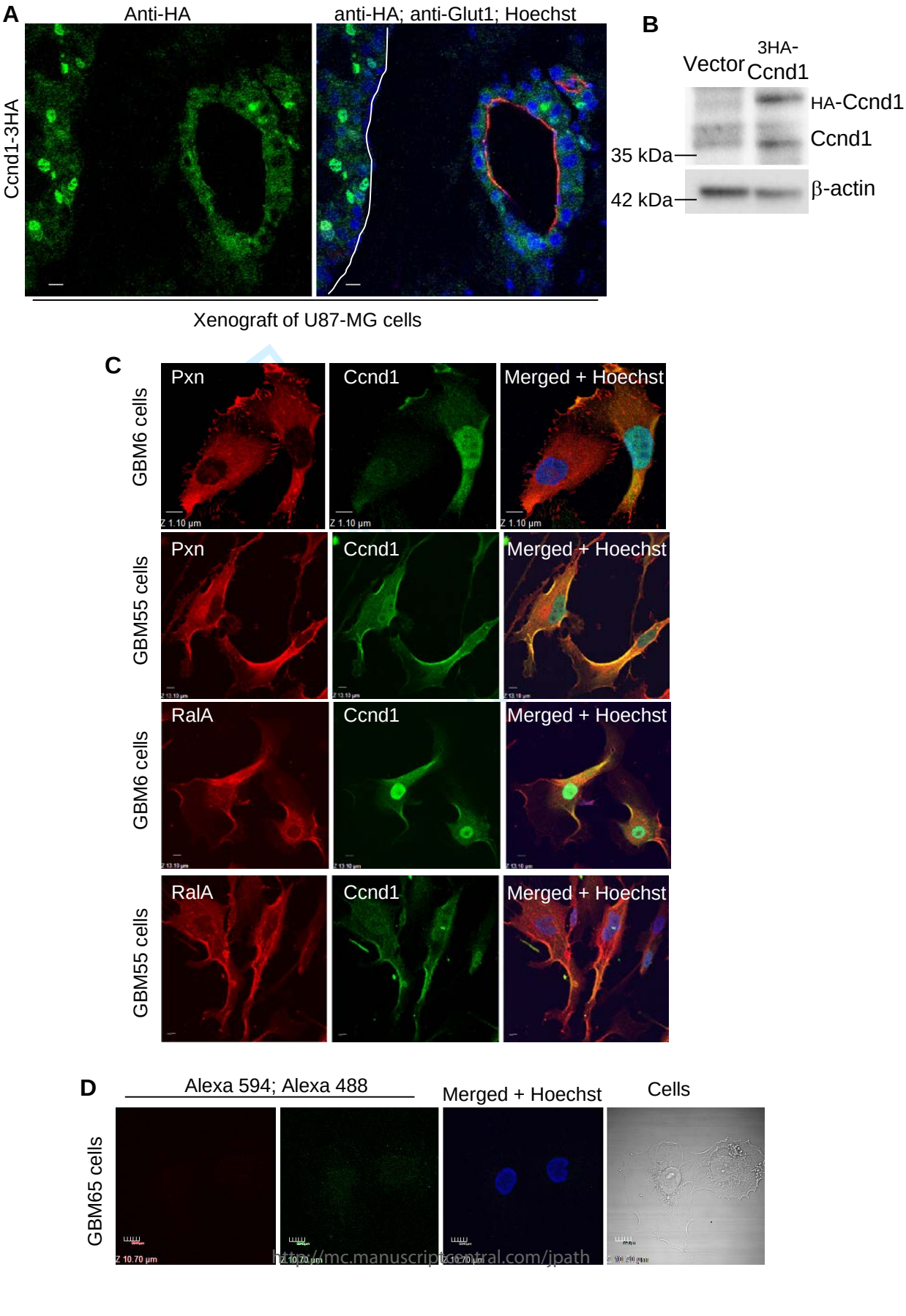

**Figure S5**

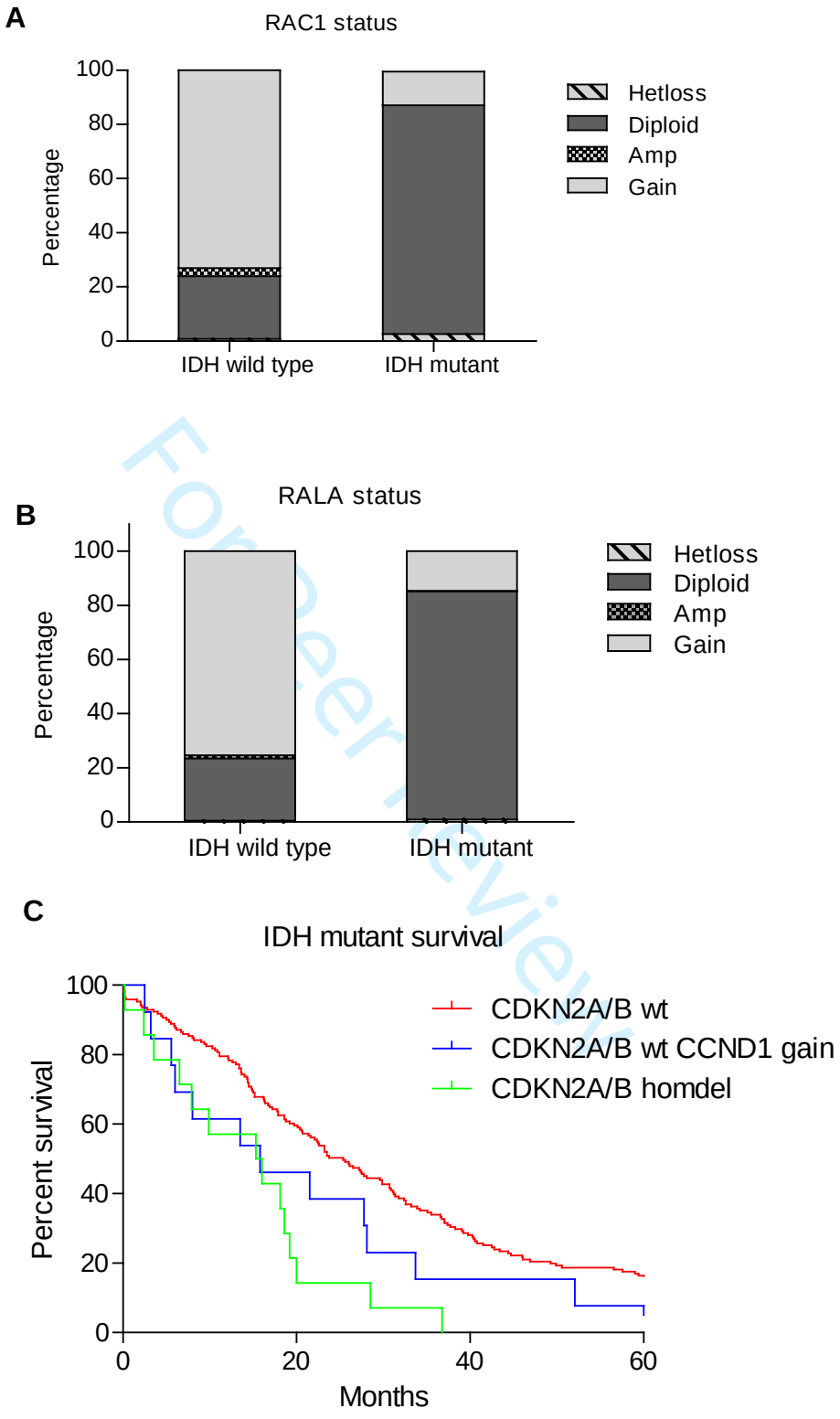

**Figure S6**

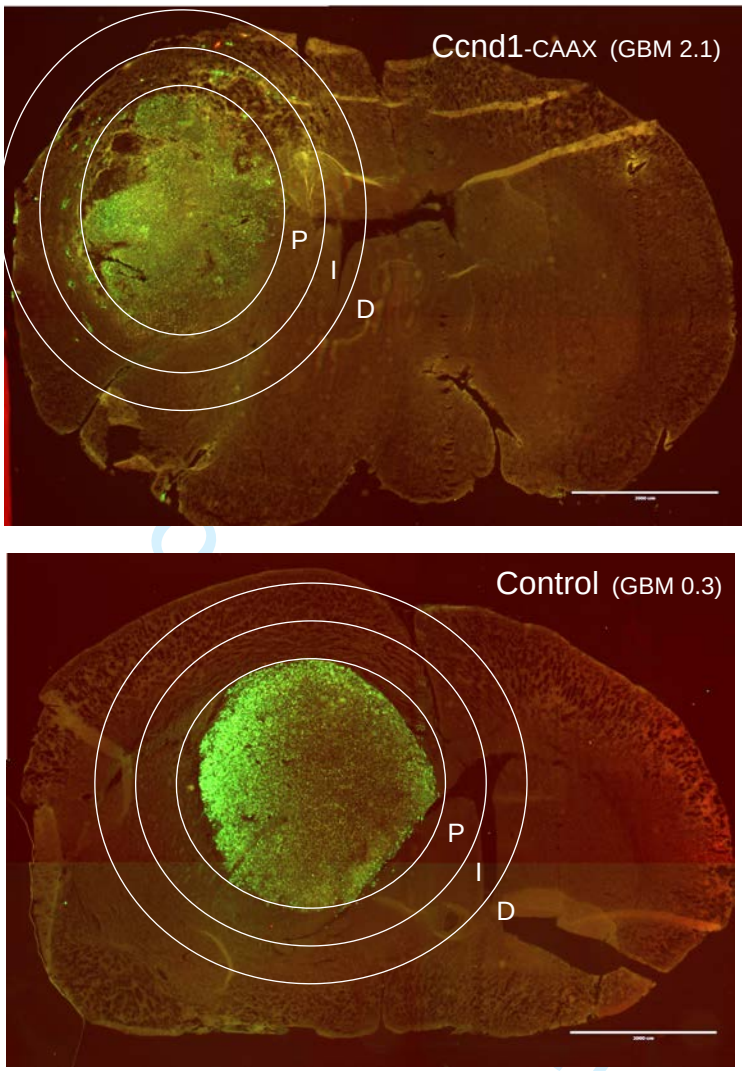
A
Ccnd1-CAAX (GBM 2.1)
P
I
D
B
Control (GBM 0.3)
P
I
D
C
Number of evaded cell foci
60
50
40
30
20
10
0
Ccnd1-CAAX
Ccnd1
Control
*
*
*
Proximal
Intermediate
Distal

**Figure S7**